Metadata, citation and similar papers at
Helsingin yliopiston digitaalinen arkisto

Atomic Layer Deposition of Multicomponent Oxide Materials

Marko Vehkamäki

Laboratory of Inorganic Chemistry
Department of Chemistry
Faculty of Science
University of Helsinki
Finland

ACADEMIC DISSERTATION

To be presented with the permission of the Faculty of Science of the University of Helsinki for public criticism in Auditorium A129 of the Department of Chemistry, A.I. Virtasen aukio, on December 21st, 2007 at 12 o'clock noon

Helsinki 2007

Supervisors

Professor Markku Leskelä
and
Professor Mikko Ritala
Department of Chemistry
University of Helsinki
Finland

Reviewers

Professor Cheol Seong Hwang
School of Materials Science and Engineering
Seoul National University
Korea

Dr. Matti Putkonen
Beneq Oy
Finland

Opponent

Professor Fred Roozeboom
Department of Applied Physics
Eindhoven University of Technology
The Netherlands

ISBN 978-952-92-3214-7 (paperback)
ISBN 978-952-10-4452-6 (pdf version)
http://ethesis.helsinki.fi

Yliopistopaino
Helsinki 2007

Abstract

Atomic layer deposition (ALD) is a method for thin film deposition which has been extensively studied for binary oxide thin film growth. Studies on multicomponent oxide growth by ALD remain relatively few owing to the increased number of factors that come into play when more than one metal is employed. More metal precursors are required, and the surface may change significantly during successive stages of the growth. Multicomponent oxide thin films can be prepared in a well-controlled way as long as the same principle that makes binary oxide ALD work so well is followed for each constituent element: in short, the film growth has to be self-limiting.

ALD of various multicomponent oxides was studied. $SrTiO_3$, $BaTiO_3$, $Ba_{(1-x)}Sr_xTiO_3$ (BST), $SrTa_2O_6$, $Bi_4Ti_3O_{12}$, $BiTaO_4$ and $SrBi_2Ta_2O_9$ (SBT) thin films were prepared, many of them for the first time by ALD. Chemistries of the binary oxides are shown to influence the processing of their multicomponent counterparts. The compatibility of precursor volatilities, thermal stabilities and reactivities is essential for multicomponent oxide ALD, but it should be noted that the main reactive species, the growing film itself, must also be compatible with self-limiting growth chemistry. In the cases of BaO and Bi_2O_3 the growth of the binary oxide was very difficult, but the presence of Ti or Ta in the growing film made self-limiting growth possible.

The application of the deposited films as dielectric and ferroelectric materials was studied. Post-deposition annealing treatments in different atmospheres were used to achieve the desired crystalline phase or, more generally, to improve electrical properties. Electrode materials strongly influenced the leakage current densities in the prepared metal–insulator–metal (MIM) capacitors. Film permittivities above 100 and leakage current densities below $1 \cdot 10^{-7}$ A/cm^2 were achieved with several of the materials.

Preface

The experimental work for this thesis was done during the years 2000–2007 in the Laboratory of Inorganic Chemistry, University of Helsinki.

I am most grateful to my supervisors Professor Markku Leskelä and Professor Mikko Ritala for their advice and guidance, and for giving me the possibility to work in the fascinating field of atomic layer deposition.

Without external contacts this work would have been limited in scale and depth. Eero Rauhala, Timo Sajavaara and Samuli Väyrynen are thanked for the ion beam analysis done at the Accelerator Laboratory. Professor Anthony C. Jones and Hywel O. Davies are thanked for the work with double-metal alkoxide precursors.

The efforts by my co-workers at the Laboratory of Inorganic Chemistry were invaluable. I would like to thank Timo Hatanpää and Timo Hänninen for preparing most of the precursors I used over the years, and Marianna Kemell for helping me with the FESEM and the electron beam evaporator.

This work would not have been possible without the support of my colleagues in the thin film group, all of whom have my gratitude. In addition to their skills and knowledge, they provided good company that helped to make this work feel meaningful.

My family and friends made life outside work enjoyable. Their encouragement and support has always helped me through the most difficult times.

Above all, I thank my wife Aino for her patience and love.

Financial support by the Finnish Funding Agency for Technology and Innovation (TEKES), Motorola, and ASM Microchemistry is gratefully acknowledged.

Helsinki, December 2007

Marko Vehkamäki

List of publications

I M. Vehkamäki, T. Hatanpää, T. Hänninen, M. Ritala and M. Leskelä. Growth of $SrTiO_3$ and $BaTiO_3$ Thin Films by Atomic Layer Deposition. *Electrochemical and Solid-State Letters* (1999), **2**(10), 504-506

II M. Vehkamäki, T. Hänninen, M. Ritala, M. Leskelä, T. Sajavaara, E. Rauhala and J. Keinonen. Atomic Layer Deposition of $SrTiO_3$ Thin Films From a Novel Strontium Precursor – Strontium bis(triisopropylcyclopentadienyl). *Chemical Vapor Deposition* (2001), **7**(2), 75-80

III M. Vehkamäki, M. Ritala, M. Leskelä, A. C. Jones, H. O. Davies, T. Sajavaara and E. Rauhala. Atomic Layer Deposition of Strontium Tantalate Thin Films from Bimetallic Precursors and Water. *Journal of The Electrochemical Society* (2004), **151**, F-69-F-72

IV M. Vehkamäki, T. Hatanpää, M. Ritala and M. Leskelä. Bismuth Precursors for Atomic Layer Deposition of Bismuth Containing Oxides, *Journal of Materials Chemistry* (2004), **14**, 3191-3197

V M. Vehkamäki, T. Hatanpää, M. Kemell, M. Ritala and M. Leskelä. Atomic Layer Deposition of Ferroelectric Bismuth Titanate $Bi_4Ti_3O_{12}$ thin films, *Chemistry of Materials*, **18**, (2006), 3883-3888

VI M. Vehkamäki, T. Hatanpää, M. Ritala, M. Leskelä, S. Väyrynen and E. Rauhala. Atomic Layer Deposition of $BaTiO_3$ Thin Films – Effect of Barium Hydroxide Formation, *Chemical Vapor Deposition* (2007), **13**, 239-246

Contents

LIST OF ABBREVIATIONS AND ACRONYMS

acac	acetylacetonate
ALD	Atomic Layer Deposition
BST	Barium Strontium Titanate
CMOS	Complementary Metal Oxide Semiconductor
CSD	Chemical Solution Deposition
CVD	Chemical Vapour Deposition
dmae	dimethylaminoethoxide
dmamp	3-N,N-dimethyl-2-methyl-2-propanoxide
DRAM	Dynamic Random Access Memory
IC	Integrated Circuit
ITO	Indium Tin Oxide
EBE	Electron Beam Evaporation
EDS	Energy Dispersive X-ray Spectrometry
Et	Ethyl
EOT	Equivalent Oxide Thickness
FEFET	Ferroelectric Field Effect Transistor
FRAM	Ferroelectric Random Access Memory
GIXRD	Grazing Incidence X-Ray Diffraction
Me	Methyl
ME	Methoxyethoxide
MIM	Metal–Insulator–Metal
MIS	Metal–Insulator–Semiconductor
MLCC	Multi-layer Ceramic Capacitor
mmp	1-methoxy-2-methyl-propanolato
MOCVD	Metal–Organic Chemical Vapour Deposition
MOD	Metal–Organic Decomposition
MOSFET	Metal–Oxide–Semiconductor Field-Effect Transistor
Ph	Phenyl
PLD	Pulsed Laser Deposition
^{i}Pr	Isopropyl
RC	Resistance–Capacitance
RF	Radio Frequency
SEM	Scanning Electron Microscope
FESEM	Field Emission Scanning Electron Microscope
PTCR	Positive Temperature Coefficient of Resistance
PZT	Lead Zirconate Titanate
RBS	Rutherford Backscattering Spectroscopy
RTA	Rapid Thermal Annealing
SBT	Strontium Bismuth Tantalate
SIS	Semiconductor–Insulator–Semiconductor
^{t}Bu	tert-Butyl
thd	2,2,6,6-tetramethylheptane-3,5-dionate
TOF-ERDA	Time-of-Flight Elastic Recoil Detection Analysis
XRD	X-ray Diffraction
XRR	X-ray Reflection

1. Introduction

Multicomponent oxide materials such as barium titanate $BaTiO_3$ and $PbZr_{(1-x)}Ti_xO_3$ (PZT) are widely used in electronics and optics. Current industrial use of these materials is typically in the form of technical ceramics. The dimensions of these ceramics components range from several micrometres in multi-layer ceramic capacitors (MLCC), to tens of micrometres in ultrasonic transducers and tunable microwave components, several millimetres in sonar transducers and several centimetres in piezo actuators. Multicomponent oxides exhibit a wide variety of material properties, such as ferroelectricity, piezoelectricity, superconductivity and electric field tunability of electrical and optical parameters.

Integrated circuits (IC) are an area where improved materials are critically needed. The rapid development of microelectronics has decreased the feature size from 1 micrometer in microprocessors in 1985 to less than 100 nm in 2007. Because of the cost and complexity of introducing new elements and chemical compounds into the IC manufacturing flow, changes in materials have been phased in only gradually. Most notably is the change to copper metallization. A more rapid rate of change will likely become necessary in the next decade. In particular, the dielectric materials SiO_2 and SiO_xN_y presently used in transistors and capacitors will need to be replaced by alternative new materials. The use of a new insulator oxide/electrode combination in the 45 nm generation transistors was, in fact, recently reported by Intel, with atomic layer deposition as the dielectric fabrication step. In future, simple reduction of the surface area of the device, or planar scaling, may need to be abandoned in favour of three-dimensional solutions. Eventually, microelectronics may need to be redesigned around new materials rather than new materials being forced into the mould of current complementary metal oxide silicon (CMOS) architecture. Future developments may thus lead to the use of thin layers of multicomponent oxide electroceramic materials in microelectronics. Ferroelectric random-access memories (FRAM) are the current state-of-the-art of electroceramics in commercial devices, but many other IC designs may benefit from electroceramics in the future. Large-area fabrication of very thin layers of multicomponent oxides continues to be challenging, which is one reason why the potential of multicomponent oxide thin films is largely untapped. The development of new and improved thin film processing methods such as atomic layer deposition is critical for enabling new multicomponent oxide applications.

The goal of this study was to develop atomic layer deposition (ALD) processes for materials that may be needed in future microelectronics, especially in memory devices, and to achieve ALD grown films with good material properties. To this end, post-deposition annealing treatments were applied to the deposited films, and Metal–Insulator–Metal capacitors were prepared in order to study the electrical properties of the films. In this work, a multicomponent oxide is considered to be a metal or semi-metal oxide compound with two or more cations and in which all the cation components are present in concentrations well above 1 atom %.

2. Background

2.1 Atomic Layer Deposition

ALD is a thin film deposition method developed by Tuomo Suntola and co-workers.[1] The original objective was to deposit large area pin-hole free dielectric–semiconductor–dielectric thin film stacks for electroluminescent displays. In ALD, thin films are grown in self-terminating reaction steps. Several benefits are associated with ALD. Film thickness can be controlled simply by adjusting the total number of self-limiting reactions. Films are typically uniform over large surface areas, from several square centimetres in small research reactors to more than 1000 square centimetres industrial scale ALD tools. Ideally they are also perfectly conformal, which not only is critically valuable in demanding IC structures,[2] but also enables the preparation of 3D nanostructures, such as vertical transistor structures [3] and inorganic nanotubes, via sacrificial templates.[4] Applications that require perfect conformality include film growth on powder samples and porous substrates. Figure 1 shows an example of a conformal $SrTiO_3$ film in a test trench. In perfectly conformal growth the thickness increases uniformly on all surfaces.

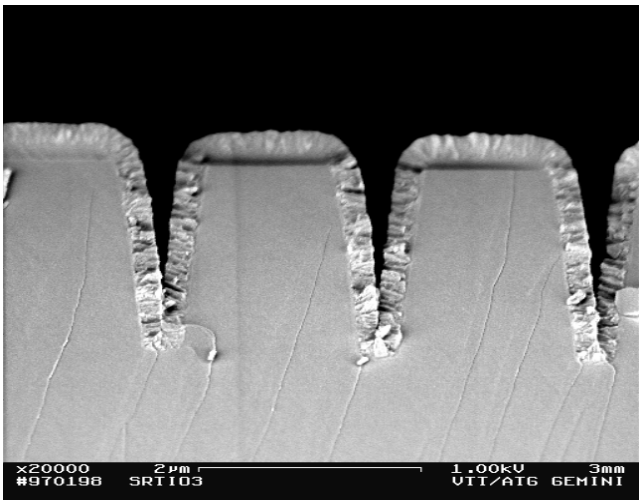

Figure 1. Conformal $SrTiO_3$ film grown on silicon test trenches.[1]

Since the 1970s, a large number of suitable ALD processes have been developed for insulating, semiconducting and conducting materials. [5] The first viable ALD

processes were those for metal oxides and compounds of other group VIa elements. The processes for metal oxides and sulfides are still the most readily applicable, as their surfaces tend to have stable reactive sites favourable to ALD growth. An example of ALD growth of MO_2 (M = Ti, Zr, Hf) is shown in Figure 2.

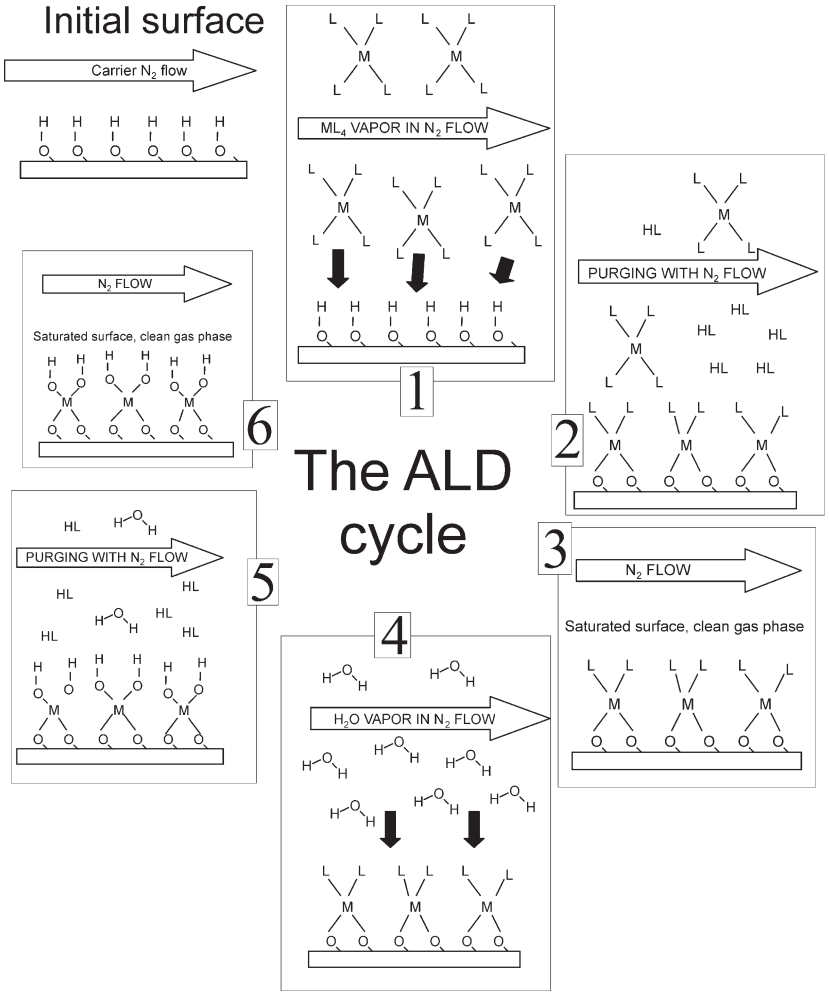

Figure 2. Schematic of ALD oxide growth, shown for MO_2 (M can be Ti, Zr, Hf) using metal precursor ML_4 (L = ligand) and H_2O as the oxygen source. Steps 3 and 6 emphasize purging, as surface saturation is often reached faster than the excess reactant and reaction products can be removed.

Initially the growth surface, for example SiO_2 or glass, is terminated with reactive –OH groups. In step **1**, the surface is exposed to a ML_4 vapour pulse, where L is a suitable ligand, for example Cl. The precursor is chosen so that it reacts quickly with the reactive surface sites, forming a stable saturated chemisorption layer. Once

saturation has been achieved, the ML_4 vapour pulse is stopped and purging begins. Step **2** presents the situation at the beginning of the purging, while step **3** shows a completed ML_4 pulse–purge sequence. The same pulse–purge sequence is repeated for H_2O vapour in steps **4** (pulse), **5** (purge onset) and **6** (completed purge), completing a full ALD growth cycle. In step **4**, the surface bonded ligands receive a proton from H_2O and leave the surface as volatile product HL, being replaced by an –OH group. The recreated –OH terminated surface is now available for the next ALD growth cycle. These cycles are repeated with each cycle adding a sub-monolayer quantity of material to the surface until a thin MO_2 film is formed. Figure 3 shows different possibilities for thin film growth rate vs. time with a metal precursor pulse in ALD of binary oxides.

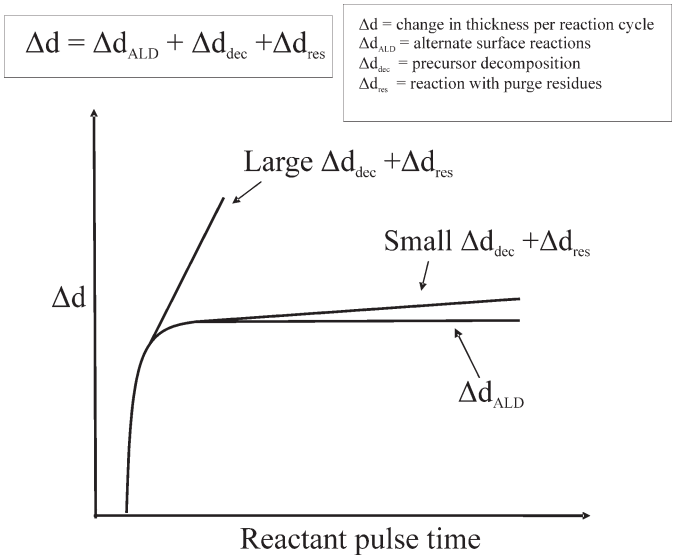

Figure 3. Self-limited growth vs. growth with undesired side reactions.

For ideal ALD, where the precursor is thermally stable and all six steps shown in Figure 2 are completed, growth self-terminates resulting in uniform and conformal increase in film thickness Δd_{ALD}. Owing to time constraints, steps **3** and **6** are sometimes skipped in actual applications of ALD. Because it is no longer ideal ALD, the **1-2-4-5** sequence results in a pulsed-Chemical Vapour Deposition (CVD) growth component Δd_{res} due to residual precursor molecules present in the gas phase. If $\Delta d_{res} << \Delta d_{ALD}$, the growth due to alternate surface reactions still dominates the overall growth rate, and the resulting film may have excellent 3D conformality. If Δd_{res} is of the

same magnitude as Δd_{ALD}, or in the extreme case where process steps **1** and **4** overlap, the surface control is lost and CVD growth takes place. In CVD-type growth the film growth rate is dominated by mass-transport of the precursor or by the reaction kinetics of the film surface. Another situation that results in non-ideal growth, even with sufficient purging, is when the metal precursor is not thermally stable at the processing temperature. A time-dependent CVD growth component Δd_{dec} due to decomposition is then added. Again, if $\Delta d_{dec} << \Delta d_{ALD}$, fairly conformal growth can be achieved, but with larger Δd_{dec} the advantages of ALD are increasingly lost. Severe decomposition of the metal precursor in the reactor can lead to precursor depletion, and further to reduced growth rate on the substrate.

Parasitic Δd_{res} and Δd_{dec} can be a serious problem with large substrate sizes such as 200–300 mm silicon wafers, and especially if deposition is done on porous substrates or powders. The necessary pulse and purge times for porous substrates and powders may be several orders of magnitude longer than those sufficient for deposition on a flat surface,[6] unless reactor setups have been specifically tailored for deposition on porous substrates.[7]

The key to developing new ALD processes is to find suitable precursor combinations which have self-limiting surface reactions. Necessary prerequisites for self-limitation in ALD of metal oxides are as follows:

I. Surface sites able to interact with the metal precursor must be present. Possible sites include reactive functionalities such as –OH groups, coordinatively unsaturated surface atoms and dissociated atomic species such as O and H.

II. The reaction of the metal precursor with the surface sites must be self-terminating with no decomposition of the precursor.

III. There must be a way to remove unreacted precursor ligands or ligand fragments left on the surface after saturation has been reached, so that a reactive surface is recreated. For oxides this means reaction with an oxygen source such as H_2O, H_2O_2, O_3, O radicals or O_2 plasma.

IV. The film must not absorb precursor species reversibly unless the absorbed species are released in an acceptably short timescale, leading to condition I.

Examples in which this condition is not met are Cu and Mo deposition processes where Zn is the reducing agent.[8]

2.2 Atomic Layer Deposition of Multicomponent Oxides

Examples of ALD growth of multicomponent oxides are listed in Table 1.[9-44, I-VI] The most straightforward and simple approach for ALD of multicomponent oxides is to use separate binary deposition cycles and adjust the composition by changing the cycle ratio. All cation precursors must be compatible, i.e. volatile, thermally stable and reactive at the same process temperature. These requirements can lead to a fairly narrow process window, or to a single optimum temperature which is just below the decomposition temperature of the least stable precursor.

Employing a separate precursor for each cation allows the highest flexibility, as films can be processed as a homogeneous mixture, a compositionally graded film or a multilayer structure with tailored interface layers simply by changing the cycle sequence. The main disadvantage of this approach is that process optimization is time-consuming. Finding the optimal growth parameters requires large numbers of deposition experiments and extensive film characterization.

A second approach is to use single-source metal precursors, that have more than one of the required cations in the same molecule (e.g. $SrTa_2(OEt)_{10}dmae_2$).[29,III] This presents the possibility to deliver the cations in the same stoichiometric ratio as in the precursor molecule, which can potentially simplify the process as there is one less precursor chemical to handle. The disadvantage is loss of composition control if dissociation or disproportionation of the double metal precursor leads to a film cation ratio different from that in the precursor molecule. Also, separate additional precursors may be needed if the optimum stoichiometry of a thin film material is different from the fixed ratio in the precursors.

Yet a third approach to growing multicomponent oxides is to use exchange reactions between an alkoxide and a halide, for example reaction between $ZrCl_4$ and $Si(OEt)_4$ to give Zr-Si-O.[36] The possibilities for composition control are limited to what naturally results from the exchange reaction, so additional binary oxide growth cycles are usually needed. The advantage of this type of processing is that oxygen source pulses and their purge steps are at least partly eliminated, making the process faster.

Although liquid injection of mixtures with all metal precursors in the same solvent, as often used in metal–organic chemical vapour deposition (MOCVD), is attractive due to the apparent practical simplicity, this is a questionable approach in ALD because the simultaneous presence of multiple precursors in the gas phase tends to cause problems. Precursors may react with one another through ligand exchange or oligomerization, which in the worst case will result in the formation of nonvolatile species. Also, different metal-organic precursors are likely to have quite different reaction kinetics, which may lead to composition profiles as precursors compete for the same chemisorption or physisorption sites on the surface. Finally, adding a solvent may increase the complexity of a process. A few reports nevertheless exist on the liquid injection of multiple precursors for ALD of multicomponent oxides.[40-44]

One key point in regard to multicomponent oxide ALD is that growth of a ternary oxide may be very different from growth of a binary oxide, and in some cases growth chemistry that works well for ternary mixtures fails for binary oxides. The reverse may also be true. For example, the growth of binary bismuth oxide is difficult, but bismuth is quite readily incorporated into mixed oxide films such as Bi-Ta-O and Bi-Ti-O. Similarly, silicon oxide (SiO_2) is difficult to grow as a binary oxide, whereas ternary silicates are readily deposited. $TiCl_4$ and H_2O are widely used for depositing TiO_2 but cannot be used for depositing alkaline earth metal titanates because MCl_2 (M = Sr, Ba) are stable and high chlorine content deposits are formed instead of a pure oxide. In certain cases, the average growth rate of a multicomponent oxide may be higher than that of the binary oxides at the same temperature, as seen, for example, for Bi-Ti-O,[V] Thus, the reactions of individual precursors are different on chemically different surfaces. ALD growth rates per cycle are usually smaller than the bonding radii of the individual atoms, so a single binary reaction cycle in a multicomponent oxide process is not sufficient to fully cover all atoms deposited in a previous cycle. Reactions should therefore be considered to take place on mixed-cation surfaces unless several consecutive ALD cycles are applied for the constituent binary oxides.

Table 1. Multicomponent oxide ALD processes reported in the literature.

Material	Precursors	References
$BaTiO_3$	$Ba(Me_5C_5)_2 + Ti(O^iPr)_4 + H_2O$ $Ba(^tBu_3C_5H_2)_2 + Ti(O^iPr)_4 + H_2O$ $Ba(^tBu_3C_5H_2)_2 + Ti(OMe)_4 + H_2O$	I, 9, IV
Bi-Si-O	$Bi(CH_2SiMe_3)_3 + O_3$	10
Bi-Ta-O	$Bi(N(SiMe_3)_2)_3 + Ta(OEt)_5 + H_2O$	IV
Bi-Ti-O pyrochlore	$Bi(Ph)_3 + Ti(O^iPr)_4 + H_2O$ $Bi(N(SiMe_3)_2)_3 + Ti(OMe)_4 + H_2O$ $Bi(mmp)_3 + Ti(O^iPr)_4 + H_2O$	11, V, 12
$Bi_4Ti_3O_{12}$	$Bi(N(SiMe_3)_2)_3 + Ti(OMe)_4 + H_2O$ $Bi(Ph)_3 + O_3 + Ti(O^iPr)_4 + H_2O$	V, 13
Bi-Ti-Si-O	$Bi(mmp)_3$, $Ti(O^iPr)_4$, $Si(OEt)_4 + H_2O$	14
Hf-Al-O	$HfCl_4$, $Al(CH_3)_3 + H_2O$ $Hf(N(C_2H_5)_2)_4 + Al(CH_3)_3 + H_2O$	15,16
Hf-Si-O	$HfCl_4 + Si(OEt)_4$ $HfI_4 + Si(OEt)_4$ $HfCl_4 + Si(OEt)_4 + H_2O$ $HfI_4 + Si(OEt)_4 + H_2O$ $HfCl_4 + H_2O + NH_2(CH_2)_3Si(OEt)_3 + O_3$	17, 18
$LaAlO_3$	$La(thd)_3 + Al(acac)_3 + O_3$	19
$LaCoO_3$	$La(thd)_3 + Co(thd)_2 + O_3$	20
$LaGaO_3$	$La(thd)_3 + Ga(acac)_3 + O_3$	21
$LaMnO_3$	$La(thd)_3 + Mn(thd)_3 + O_3$	22
$LaNiO_3$	$La(thd)_3 + Ni(thd)_3 + O_3$	23
$MgAl_2O_4$	$Mg(C_5H_5)_2 + Al(CH_3)_3 + O_3$	24
$NdAlO_3$	$Nd(thd)_3 + Al(CH)_3 + O_3$	25
$PbTiO_3$	$Pb(Ph)_4 + O_3 + Ti(O^iPr)_4 + H_2O$ $Pb(dmamp)_2 + H_2O + Ti(O^tBu)_4 + H_2O$	26, 27

$PbZrO_3$	$Pb(Ph)_4 + O_3 + Zr(thd)_4 + O_3$	28
$SrBi_2Ta_2O_9$	$SrTa_2(OEt)_{10}dmae_2 + H_2O$ + $Bi(N(SiMe_3)_2)_3 + H_2O$	IV
$SrTa_2O_6$	$SrTa_2(OEt)_{10}dmae_2 + O_2$ plasma $SrTa_2(OEt)_{10}dmae_2 + H_2O$	29, III
$SrTiO_3$	$Sr(^iPr_3C_5H_2)_2 + Ti(O^iPr)_4 + H_2O$ $Sr(MEthd)_2 + Ti(O^iPr)_4 + O_2$ remote plasma $Sr(thd)_2 + O_3 + Ti(O^iPr)_4 + H_2O$ $Sr(thd)_2 + Ti(O^iPr)_4 + H_2O$ remote plasma	I,II, 30,31,32
Ta-Al-O	$TaCl_5 + AlCl_3 + H_2O$	33
$Ta_{(1-x)}Nb_xO_5$	$Ta(OEt)_5 + Nb(OEt)_5 + H_2O$	34
$YScO_3$	$Y(thd)_3 + Sc(thd)_3 + O_3$ $Y(MeC_5H_4)_3 + Sc(Cp)_3 + H_2O$	35
Zr-Al-O	$ZrCl_4 + Al(OEt)_3$ $ZrCl_4 + Al(CH_3)_3 + H_2O$	36, 37
Zr-Si-O	$ZrCl_4 + Si(OEt)_4$ $ZrCl_4 + Si(O^nBu)_4$ $ZrCl_4 + H_2O$ + $NH_2(CH_2)_3Si(OEt)_3 + O_3$	36, 38
Zr-Ti-O	$ZrCl_4 + Ti(O^iPr)_4$	36, 39
$Bi_4Ti_3O_{12}$	$Bi(mmp)_3$ and $Ti(mmp)_4$ in ethylcyclohexane + O_3/O_2	40
Bi-Ti-Al-O	$Bi(mmp)_3$, $Ti(mmp)_4$ in ethylcyclohexane, $Al(CH_3)_3 + H_2O$	41
Bi-Ti-Si-O	$Bi(mmp)_3$, $Ti(mmp)_4$ and $Si(OEt)_4$ in ethylcyclohexane + O_3	42
$SrTiO_3$	$Sr(tmhd)_2$ and $Ti(O^iPr)_4$ in tetrahydrofurane + O_2 plasma	43
$SrBi_2Ta_2O_9$	$Bi(Ph)_3$ and $SrTa_2(OEt)_{10}ME_2$ in n-butylacetate + O_2 plasma	44

2.3 Dielectric and Ferroelectric Materials

Dielectric materials are used for both charge separation and charge accumulation in solid state structures.[45,46] Charge separation requires sufficiently insulating materials, that is, materials having a high resistivity or low conductivity. Leakage current through a dielectric material is the main limitation on its application. The main factors influencing the leakage current are the band gap of the material, properties of the dielectric/electrode interface, nonstoichiometry, impurities, vacancies and crystallinity.

The band gap is the energy difference between the valence and conduction bands in a material. Materials with a band gap larger than 5 eV are considered to be good insulators, but many materials that are candidates for dielectrics in future microelectronics (e.g. $SrTiO_3$) have band gaps in 3-5 eV range. For low band gap dielectric materials, the electronic work function of the electrode material and the quality of the interface (e.g. roughness and density of trap states) often limit the leakage current, as for example in $Ba_{(1-x)}Sr_xTiO_3$. Oxygen vacancies serving as donors are often responsible for high electronic conduction in oxides. Impurities can also act as acceptors or donors, thereby influencing leakage current. Film microstructure also affects the leakage; for example, polycrystalline thin films can be electrically very heterogeneous, with the grain boundaries causing either increased or reduced electrical conduction.

The use of dielectric materials for charge accumulation depends on the polarizability of the dielectric. The polarizability of a dielectric can have electronic, ionic, and boundary layer contributions depending on the elemental composition and structure of the material. Different polarization mechanisms respond differently to signal frequency. When a dielectric material is placed between two electrode plates, an electrical element called a capacitor is formed. When a voltage difference U is applied between the electrodes, an excess of electronic charge Q- collects on the negatively biased capacitor plate, and a corresponding opposite charge Q+ on the positively charged capacitor plate until the voltage drop across the dielectric is equal to the voltage difference from electrode to electrode. The capacitor is then fully charged. The saturated charge of a capacitor is equal to

1) $$Q = C \cdot U$$

The quantity C is the capacitance in farads (F) and U is the applied voltage. The capacitance of a plate capacitor is equal to

2) $C = \varepsilon_0 \varepsilon_r A/d$

Here ε_0 is the permittivity of vacuum ($8.815 * 10^{-12}$ F/m), ε_r is the relative permittivity which is a unitless quantity used to compare the permittivity of a medium with that of vacuum, A is the surface area of the smaller electrode, and d is the thickness of the dielectric.

Three types of dielectrics are relevant in this study, namely linear dielectrics, nonlinear dielectrics and ferroelectrics. In linear dielectrics the permittivity of the material is largely independent of the applied electric field, although minor variation may occur, which results in a linear accumulation of charge as the electric field is increased (see Figure 4a). Nonlinear dielectrics have a field-dependent permittivity, which causes a deviation from linear Q-V behaviour (Figure 4b). Ferroelectrics are materials that have a Q-V hysteresis due to a remanent polarization below their Curie temperature T_c (Figure 4c).

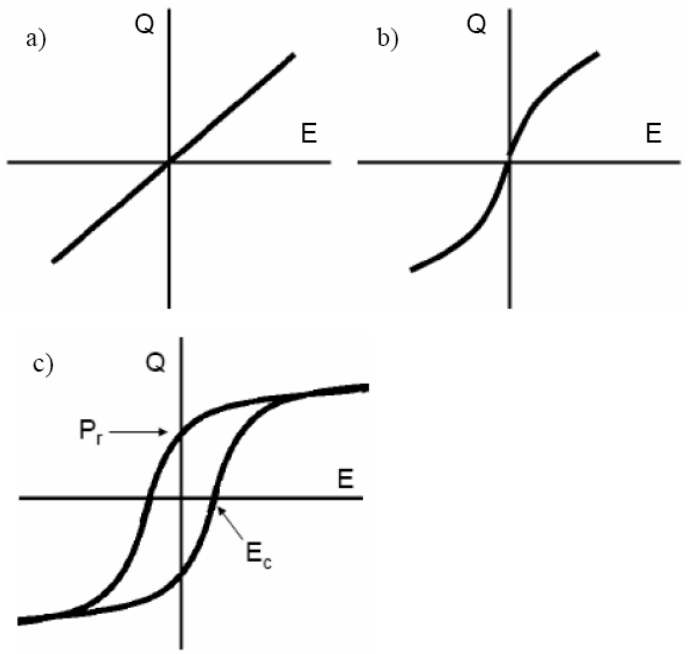

Figure 4. The charge as a function of applied electric field for a) linear, b) nonlinear, and c) ferroelectric capacitors.

Ferroelectrics have two non-zero polarization states, the direction of which can be switched by applying a sufficiently high electric field called the coercive field, E_c. The remanent polarizations, $\pm P_r$, which remain after the external electric field is removed, can be used in memory devices to denote logic states 0 and 1. Some examples of linear, nonlinear and ferroelectric materials are given in Table 2. Ferroelectricity exists due to the noncentrosymmetric crystal structures of the materials (See section 2.4)

The electrical properties of multicomponent oxides tend to be highly complex. Processing an ideally stoichiometric multicomponent oxide material is difficult by any method, and some excess of one of the cations should always be considered to be present in a multicomponent oxide system. The permittivities and resistivities of multicomponent oxides are highly sensitive to the cation composition and film microstructure, which is one of the main difficulties in applying these materials as dielectrics in microelectronics. The permittivities of high dielectric constant materials often decrease dramatically with decreasing film thickness, which is often called the intrinsic dead layer effect. A low capacitance layer in series with the dielectric capacitance has often been regarded as the cause for this decrease. This series capacitance has been considered to be due to either a lower dielectric constant interface layer in the dielectric surface or an electrode capacitance. An electrode capacitance may result from the finite free electron density of the electrode materials which causes a finite charge screening length in the electrode.[47] Recent work suggests that the charge screening length is the dominant cause for the dead layer effect and that the fabrication of the electrode material can be the critical step in capacitors with ultra-thin dielectric layers.[48]

Table 2. Permittivities of selected oxide materials.

Dielectric material	Relative permittivity	Dielectric type
SiO_2	3.9	Linear
SiON	7	Linear
Al_2O_3	7–9	Linear
Ta_2O_5	20–25	Linear
Amorphous $SrTiO_3$	14–15	Linear
$SrTiO_3$ single crystal	330	Nonlinear
Amorphous $BaTiO_3$	15–17	Linear
Crystalline $BaTiO_3$	2500 (ceramic)	Nonlinear, Ferroelectric below T_c=393 K
Crystalline $Bi_4Ti_3O_{12}$	120–200 (anisotropic)	Nonlinear, Ferroelectric below T_c= 948 K

2.4 Structures of Multicomponent Oxides

There are vast possibilities for varying the structure, chemical composition and resulting material properties of multicomponent oxides. For example, perovskite dielectric $SrTiO_3$ can be doped with Nb to make it conductive, or the dielectric properties of $Ba_{(1-x)}Sr_xTiO_3$ can be adjusted between paraelectric and ferroelectric by changing the Sr content. Most of the interesting material properties, such as dielectric permittivities > 100, ferroelectricity, piezoelectricity and superconductivity, to name a few, require a specific crystalline phase of a multicomponent oxide.

Amorphous oxide mixtures prepared at low temperature are often used as intermediates in preparing crystalline oxides. Amorphous multicomponent oxides often form because of kinetic reasons or as a result of the low temperature used in their preparation. Even though a crystalline phase is the most stable species in an oxide system, the rearrangement of bonds and atomic positions required for the formation of a crystal lattice often requires high temperatures. Thin films of amorphous multicomponent oxides can be crystallized by thermal annealing, and in some cases even epitaxial films result.[49]

The oxidation states and effective ionic sizes of the constituent elements are key factors influencing the solid state structures. On the basis of structural data of oxides and halides, Shannon[50] compiled a comprehensive list of the effective ionic radii for different coordination numbers, as shown in Table 3 for selected elements.

Table 3. Effective ionic radii vs. coordination number for selected ions.[50]

	CN 4	CN 5	CN 6	CN 8	CN 12
Calcium (II)			1.00 Å	1.12 Å	1.34 Å
Strontium (II)			1.18 Å	1.26 Å	1.44 Å
Barium (II)			1.35 Å	1.42 Å	1.61 Å
Bismuth (III)		0.96 Å	1.03 Å	1.17 Å	
Titanium (IV)	0.42 Å		0.605 Å		
Zirconium (IV)	0.59 Å	0.66 Å	0.72 Å	0.84 Å	
Hafnium (IV)	0.58 Å		0.71 Å	0.83 Å	
Niobium (V)	0.48 Å		0.64 Å	0.74 Å	
Tantalum (V)			0.69 Å	0.74 Å	
Oxygen (-II)	1.38 Å		1.40 Å	1.42 Å	

The most important multicomponent oxide structures encountered in the present work are introduced in sections 2.4.1−2.4.5

2.4.1 Solid solutions

Perhaps the simplest type of multicomponent oxide is a substitutional solid solution, in which two metals can occupy the same metal ion site in the structure. Binary oxides that form a full solid solution range must be isostructural and chemically sufficiently similar: similar ionic radii, similar electronegativity and identical charge. Examples of solid solutions include $Ta_{(1-x)}Nb_xO_5$, which is a mixture of Ta_2O_5 and Nb_2O_5, and $Hf_{(1-x)}Zr_xO_2$. Ternary oxides can also form a solid solution, for example perovskites $SrTiO_3$ and $BaTiO_3$ form $Ba_{(1-x)}Sr_xTiO_3$.

Other types of solid solutions besides full solid solutions include limited range solid solutions, interstitial solid solutions and amorphous solid solutions. Limited range solid solutions are more common than full solid solutions, and in multicomponent oxides there is considerable substitutional chemistry available to modify the structure.[51] Interstitial solid solutions of a multicomponent oxide and an impurity, such as hydrogen, can form during material processing, for example with $BaZrO_3$.[52,53] Amorphous solid solutions, often formed at low temperature, enable solubility of constituent oxides and/or impurities which that would segregate from a crystalline mixture. Glasses are an important example of amorphous multicomponent oxide solid solutions.

2.4.2 Perovskites

The perovskite structure [54] ABX_3, named after the mineral perovskite $CaTiO_3$, is common when two cations of sufficiently different size form a lattice with an oxide, a chalcogenide or a halide anion. More exotic examples, such as perovskite hydrides, exist as well.[55] In a perovskite structure the A cations are twelve-coordinated and the B cations six-coordinated. The cubic perovskite structure of $SrTiO_3$ is shown in Figure 5. Although the structure is in principle simple, the possible in variations in crystallographic structure, cation composition and/or cation and anion vacancies provide a huge variety of physical properties. An example of structural variation is the change of the crystalline phase from orthorhombic in $CaTiO_3$ to cubic in $SrTiO_3$, and finally to tetragonal in $BaTiO_3$, as the size of the group II metal increases. For comparison, in $MgTiO_3$ all cations are six-coordinated. Many perovskites, for example $BaTiO_3$ and

$SrTiO_3$, have a large dielectric permittivity because ionic displacements can readily take place in the perovskite lattice. $CaTiO_3$ and $SrTiO_3$ are paraelectric even at low temperature,[56, 57] and $BaTiO_3$ has a ferroelectric transition at T_c=393 K. Ferroelectricity can be induced in $SrTiO_3$ by doping or by applying external stress, so $SrTiO_3$ is considered to be an incipient ferroelectric.[58] $BaTiO_3$ is a text-book example of a ferroelectric material.[54] Ferroelectricity in $BaTiO_3$ arises from displacement of the anion and cation sublattices with respect to each other. The smaller titanium atom is displaced to a larger extent than Ba.[59]

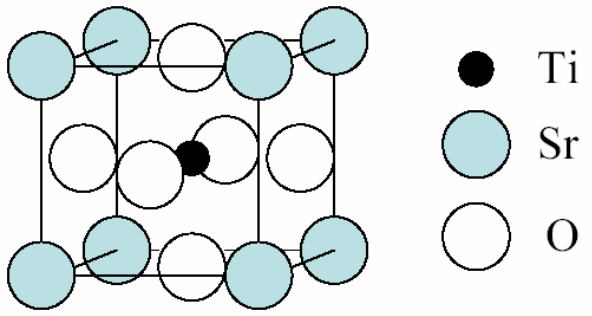

Figure 5. Cubic perovskite $SrTiO_3$

2.4.3 Layered perovskites

Layered perovskite compounds consist of perovskite-like units separated by differently organized layers. Layered perovskites are found in various chemical systems, for example, superconducting copper oxide layered perovskites, such as $YBa_2Cu_3O_{(7-\delta)}$, and bismuth oxide layered perovskites, often called Aurivillius phases.[60] Layered perovskites have perovskite-like layers sandwiched between bismuth oxide layers: $BaTa_2O_7^{2-}$ layers between $Bi_2O_2^{2+}$ planes in $BaBi_2Ta_2O_9$, for example, as shown in Figure 6. In $BaBi_2Ta_2O_9$ the bismuth atoms form an eight-coordinated square antiprism with shorter distances to the four oxygen atoms in the $Bi_2O_2^{2+}$ planes and longer distances to the oxygen atoms in the perovskite layer. Ba and Ta have perovskite-type 12-fold and 6-fold coordination, respectively. The preference of bismuth for asymmetrical bonding strongly influences the Aurivillius oxide structures, and also the structures of other bismuth-containing oxides. This is generally considered to be due to

the influence of the stereochemically active $6s^2$ electrons. The same inert pair effect is present in the solid state chemistry of Sn, Sb, Tl and Pb.

As shown in a study by Shimakawa et al. [61] of $M^{II}Bi_2Ta_2O_9$, (M^{II} = Ca, Sr, Ba) phases, the structure is most ordered with Ba, where there is a broad relaxor ferroelectric type maximum of permittivity at T_c=60 °C. The lattice mismatch between the perovskite and $Bi_2O_2^{2+}$ layers increases as the size of the M^{II} cation decreases, causing distortion in the TaO_6 octahedra and increasing the T_C to about 300 °C for $SrBi_2Ta_2O_9$ (SBT) and above 600 °C for $CaBi_2Ta_2O_9$. Note that this is opposite to the trend in perovskite titanates, underscoring the difference in the polarization mechanisms of $BaTiO_3$ and SBT.

The reversible ferroelectric polarization in SBT is a combination of rotation of TaO_6 octahedra and displacement of Bi atoms in the $Bi_2O_2^{2+}$ layer, both parallel to the a-b plane.[62] This means that the ferroelectric polarization occurs only in the direction of the a-b plane. The further result is anisotropy of the dielectric properties, so that the material acts as a ferroelectric when an electric field is applied parallel to the a-b plane and as a paraelectric when the field is applied parallel to the c-axis. Bismuth atoms can occupy the M^{II} site in SBT, causing structural distortion at the twelve-coordinated site. When Bi was substituted for Sr by Shimakawa et al.[62] to form $Sr_{0.8}Bi_{2.2}Ta_2O_9$, the resulting Sr site occupancies were 82% Sr and 12% Bi, with 6% vacancies. The vacancies helped to maintain the overall charge neutrality of the structure as no extra oxygen was observed. The ferroelectric transition shifts upwards to 400 °C due to the increased distortion caused by Bi in the perovskite block.

In the layered perovskite bismuth titanate $Bi_4Ti_3O_{12}$ (Figure 7) the bismuth atoms are split into two groups with half of them, Bi(2), in the Bi_2O_2 layer and the other half, Bi(1), in the perovskite layer. There are three vertically stacked TiO_6 octahedra in the unit cell, with two slightly differently bonded Ti sites: Ti(1) in the TiO_6 octahedra that are not in contact with the $Bi_2O_2^{2+}$ layer, and Ti(2) in the TiO_6 octahedra that are.[63, 64] Below the Curie temperature of 675 °C the coordination spheres of the cations, especially Bi(1), are asymmetrically distorted. This is the main cause of the ferroelectricity in $Bi_4Ti_3O_{12}$. $Bi_4Ti_3O_{12}$ differs from SBT in that there is a ferroelectric polarization component in the c-axis direction. $Bi_4Ti_3O_{12}$ single crystals have remanent polarizations of 4 and 50 $\mu C/cm^2$ in the a-b plane and c-axis directions, respectively.

Above the Curie temperature the distortions are eliminated by thermal motions, and the structure changes to tetragonal and centrosymmetric.

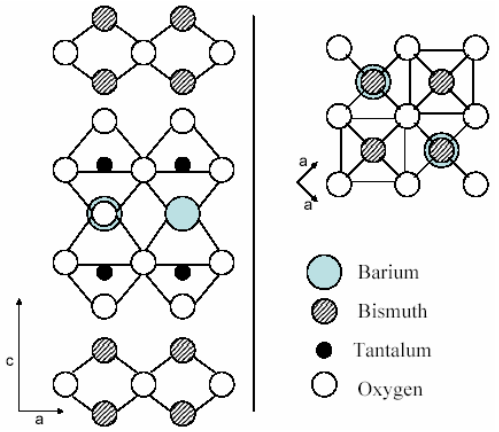

Figure 6. Example of a layered perovskite structure. The structure shown is tetragonal $BaBi_2Ta_2O_9$, presentation after Shimakawa.[61] The coordination is 12-fold for Ba and 6-fold for Ta which is similar to a perovskite structure.

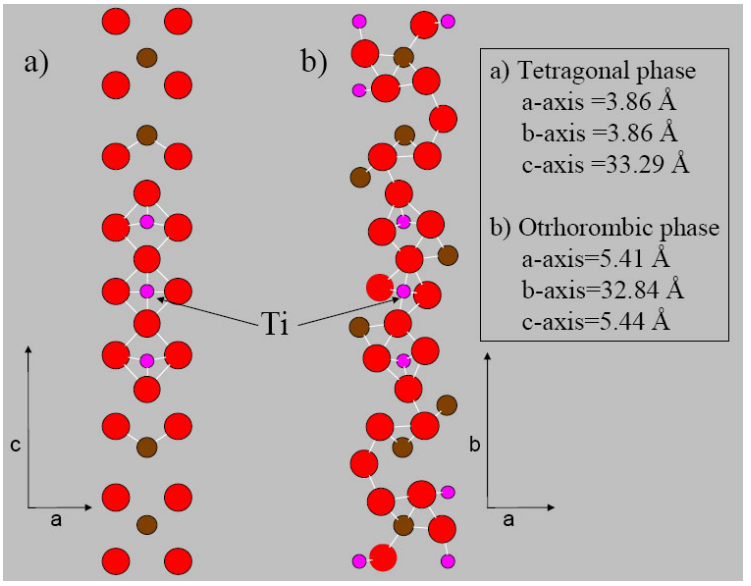

Figure 7. Cross-sections of $Bi_4Ti_3O_{12}$ structure demonstrating the distorted Ti atom coordination: a) high-temperature nonferroelectric tetragonal phase in a-c plane at b=0, viewed along the b axis and b) room-temperature ferroelectric phase viewed along the c-axis, with atoms shown from -0.2 c to 0.3 c. Atomic coordinates from ref. 63.

Recently the partial replacement of bismuth with lanthanum was found to improve the material properties of $Bi_4Ti_3O_{12}$.[65] When 18.75% of the Bi is replaced with La (radius of 1.36 Å with CN 12) to give $Bi_{3.25}La_{0.75}Ti_3O_{12}$, the lanthanum is accommodated solely in the perovskite layer.[64] Hervoches et al.[66] observed that with larger substitutions, lanthanum becomes disordered, partly occupying cation positions in the $Bi_2O_2^{2+}$ layer, with 6% and 21% populations in $Bi_3LaTi_3O_{12}$ and $Bi_2La_2Ti_3O_{12}$, respectively. Since part of the asymmetrically bonding bismuth in the perovskite block is replaced by lanthanum, the distortions in the perovskite site correspondingly decrease. This causes the Curie temperature to drop from 675 °C to 396 °C for $Bi_{3.25}La_{0.75}Ti_3O_{12}$, which corresponds to a 25% substitution at the perovskite site. Simultaneously the polarization in the c-axis direction is slightly increased.

2.4.4 Fluorites

Fluorite structures, named after the mineral fluorite CaF_2, have an 8-coordinated cation site, and the anions adopt a tetrahedral coordination (Figure 8). Examples of fluorite structured oxides include CeO_2, metastable cubic ZrO_2, lanthanide-doped cubic ZrO_2, BiO_2 (Bi III-Bi V) and $Bi_{3.2}Mo_{0.8}O_{7.5}$. The fluorite structure is also encountered in multicomponent oxides at low-temperature, for example in $SrBi_2Ta_2O_9$.[67-68] The cations in fluorite SBT may be ordered because Ta(V) has a much smaller 8-coordinate ionic radius than Sr and Bi (Table 3), and Bi $6s^2$ lone pairs need to be accommodated in the structure. Evidence for cation ordering in fluorite SBT was seen by Lee et al. [69] in epitaxial pulse laser deposited SBT films. Rodriguez et al.[68] showed that cation ordering was different for powder and thin film samples of Sr-Bi-O fluorite. The powder sample consisted of hexagonally packed fluorite-like sheets separated by layers with Bi $6s^2$ lone pair electrons and partially occupied oxygen sites, but in Sr-Bi-O thin films possessed a simple cubic fluorite structure. The mechanical stress present in the thin film samples was suggested as a possible reason for the difference. Fluorite SBT has been considered as a beneficial intermediate phase for the formation of the layered perovskite SBT structure.[68, 70]

2.4.5 Pyrochlores

The pyrochlore structure $A_2B_2O_7$, named after the pyrochlore minerals, is related to the fluorite structure (Figure 9). The larger A cations are eight-coordinated, and the smaller B cations form BO_6 octahedra. One of the seven oxygen ions is bound only to A cations.[71] Bismuth-containing pyrochlores often have structures with a high degree of disorder especially with respect to the positions of the bismuth ions. The stereochemical effect of bismuth $6s^2$ electrons probably contributes to this. Pyrochlore phases are found in both Sr-Bi-Ta-O and Bi-Ti-O systems. Bismuth deficient pyrochlore SBT [72] is often encountered in thin film structures.[73] Phase-pure $Bi_2Ti_2O_7$ easily decomposes to other bismuth titanates and it was only recently synthesized.[74] The structure is stabilized by the presence of excess titanium [75] or by replacing part of the Bi and Ti with other cations.[76]

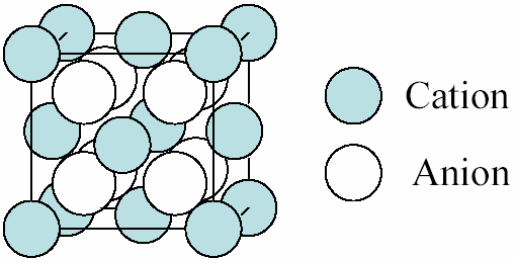

Figure 8 The fluorite structure. In the mineral fluorite CaF_2, calcium has f.c.c. packing and fluorine simple cubic packing. The cations form an eight-coordinated cubic array and the anions have a four-coordinated tetrahedral arrangement.

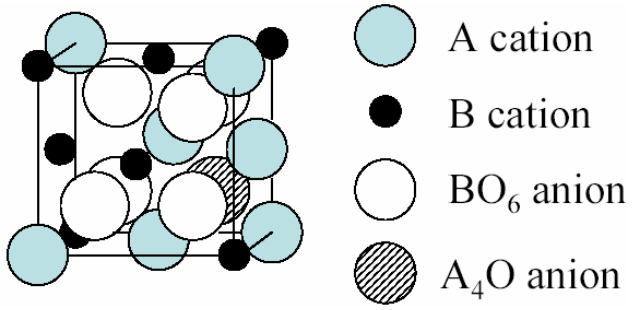

Figure 9. Simplified presentation of the cubic pyrochlore structure. Only 1/8 of the pyrochlore cell is shown. The cations have the same f.c.c. packing as in the fluorite structure. One of the anion sites is empty and one of seven anions is bound to A site cations only. In reality the BO_6 anions are all displaced with respect to anion positions in the fluorite structure.

2.5 Metal–Insulator–Metal and Metal–Ferroelectric–Metal Capacitors

Capacitors act as reservoirs of electrical energy. A Metal–Insulator–Metal (MIM) capacitor is a stack with a dielectric film between two electrode films. For MIM capacitors, the metal is considered to be any metallic conductor, including conductive nitrides such as TaN and TiN and oxides such as RuO_2 and IrO_2. MIM capacitors are used in applications such as charge storage for memory [77,78] and for decoupling. Decoupling capacitors are placed around integrated circuits to protect them from drops in the operation voltage.[79,80]

MIM capacitors can be expected gradually to replace SIS [2] and MIS [81] capacitor structures because problems with interfacial SiO_2 formation are avoided and they allow the possibility of limiting the leakage current by creating or enhancing an interface Schottky barrier. The interface barrier improves the performance of lower band gap dielectrics such as perovskite titanates. High capacitance density, low leakage current and reliability are all important for MIM capacitor performance. Compared with binary oxides and nitrides, it is easier to reach high capacitance densities with multicomponent oxides due to their high permittivities, but to simultaneously obtain low leakage and sufficient capacitor lifetime is much more challenging. The electrodes should have sufficiently low resistivity to avoid RC delays, and the low resistivity must be retained during capacitor processing and all following processes. Also, the electrodes can act as a template for getting a beneficial microstructure in crystalline dielectrics, so their structure and surface morphology should be well controlled.

The three main types of MIM capacitors are planar, 3D stacked and trench (Figure 10). The planar capacitors are the simplest to fabricate, but least area-efficient, i.e., they have the highest footprint area per given unit capacitance. Stack capacitors rely on 3D electrodes to increase total capacitance per unit wafer area, and trench capacitors take the area enhancement to the extreme with very high aspect ratio >10:1 structures.

In all types of MIM the highest possible capacitance density at an acceptable leakage current density is desired. Because of the historical significance of SiO_2 in IC development, the capacitance density of a capacitor is often reported as SiO_2 equivalent oxide thickness (EOT). EOT = $(3.9/\varepsilon_r)\cdot d$, where ε_r and d are the permittivity and thickness of the dielectric material. EOT indicates the SiO_2 thickness that would give the same capacitance density as the dielectric under study. EOT values less than 1.0 nm

are already needed in present microelectronics, as transistor gates in high performance microprocessors require charge densities of this magnitude. Memory capacitors will also require similar charge densities in the near future.

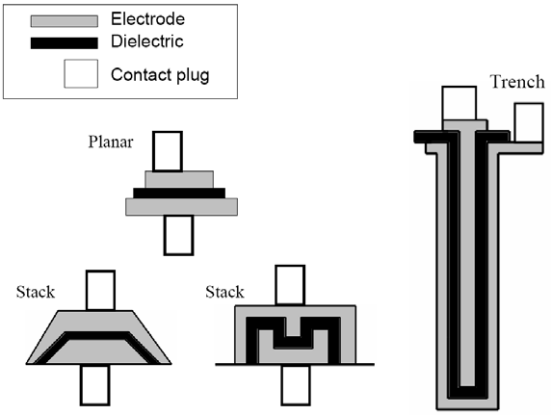

Figure 10. Different thin film capacitor geometries.

Metal–Ferroelectric–Metal (MFM) capacitor structures are MIM capacitors in which the dielectric has a ferroelectric polarization component in the direction of the applied electric field. Noble metals and noble metal oxides RuO_2 and IrO_2 are the most suitable materials for MFM electrodes as they survive O_2 annealing well. The metal–ferroelectric interface is critical for reducing fatigue and imprint. Fatigue means the reduction of the remanent polarization during continued switching, and imprint is the irreversible freezing of the polarization in one direction. Integration of ferroelectric capacitors into silicon electronics requires highly specialized electrode structures with built-in oxygen barriers and carefully controlled stress.

2.6 Dynamic Random Access Memory

Dynamic random access memory (DRAM) is currently the most important type of memory in modern computers. The highest density DRAM consists of single-transistor, single-capacitor (1T1C) memory cells (Figure 11). Single cells are arranged in a rectangular array and are connected by conductors called word and bit lines.[82] The cells are accessed by biasing the word line in contact with gates of the access transistors of given cells. This opens the transistor channel for charging and discharging of the capacitor through the bit line. Binary states 0 and 1 are defined by two voltage levels

and the corresponding charges in the capacitor. Because of the simple structure, scaling of DRAM to high memory densities was relatively straightforward during the twentieth century, but an increase in geometric and material complexity is now in progress. DRAM cells have short access times, which makes them good complements to high speed microprocessors. When the supply voltage is turned off the information will dissipate within a few seconds, making DRAM a volatile memory. Due to capacitor leakage, a refresh circuit needs to re-write the stored information in a refresh cycle, which is repeated after each 64 ms or less — hence the name dynamic.

There are two main types of DRAM capacitor structures: stacked [83] and trench.[84] In the stacked DRAM, the transistors are fabricated before capacitors, which places thermal budget limits on the capacitor fabrication. In trench DRAM the capacitors are made before transistors, so the capacitors must survive the implant activation annealing (>1000 °C). Previously, doped polysilicon was used for both bottom and top electrodes, but a transition to MIS and finally to MIM structures is underway, as this eliminates the interface oxidation and depletion problems associated with the dielectric-polysilicon interfaces. The fabrication of MIM structures for trench DRAM also makes the development of ALD processes for both the electrodes and the dielectrics highly important.

2.7 Ferroelectric Random Access Memory

Ferroelectric random access memory (FRAM) uses an MFM capacitor combined with one or more transistors to make a memory array similar to a DRAM.[85] The key difference is that the memory is nonvolatile and information is retained when the power is turned off. Ferroelectric memories have matured to IC mass production fairly recently, but integration densities remain far behind those of DRAM. The main challenges have been to develop processes compatible with current IC processes and to avoid ferroelectric fatigue during FRAM operation. FRAM is interesting because it offers a way toward a universal nonvolatile memory. FRAM can be accessed fast and can be operated at lower voltage than flash memories. Commercial FRAM memories are available with $PbZr_{(1-x)}Ti_xO_3$ (PZT) and $SrBi_2Ta_2O_9$ (SBT) ferroelectrics. With PZT the electrode materials vary, but usually at least one oxide electrode, such as RuO_2, IrO_2

or $SrRuO_3$, is usually included in order to increase the device lifetime. In SBT-based memories Pt electrodes are used in contact with the ferroelectric.

Another type of FRAM under study is the Ferroelectric Field-effect Transistor (FEFET), in which a ferroelectric material is used as a gate dielectric in a Metal–Oxide–Semiconductor Field-effect Transistor (MOSFET) gate stack. The logic states 0 and 1 are defined by two transconductance levels caused by the ferroelectric polarization of the gate insulator stack. This is a single component memory, in which the read operation does not require change in the ferroelectric polarization state. The main challenge is to find a reliable combination of buffer dielectric and ferroelectric film, a task that has proven difficult.[86]

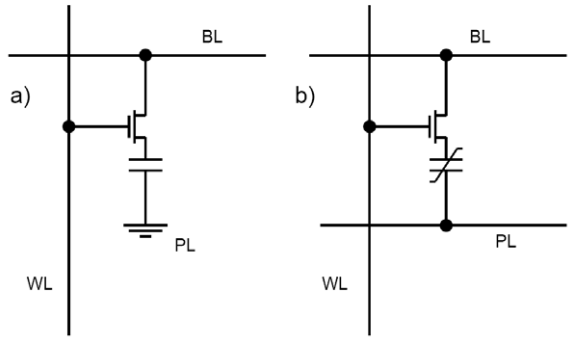

Figure 11. Layout of a) a 1–transistor–1–capacitor DRAM and b) a 1–transistor–1–capacitor FRAM cell. BL, WL and PL stand for bit line, word line and plate line, respectively. The differences are in the type of capacitor and plate line voltage levels. In DRAM the plate line is grounded or at constant voltage, whereas in FRAM the plate line voltage is varied in order to switch the ferroelectric capacitor.

3. Experimental

3.1 Film Growth

All ALD experiments of this work were made in flow-type F120 ALD reactors operated with chamber pressures of roughly 10 mbar.[1] Nitrogen carrier gas of 99.999% or better purity was used for purging and pulsing of the precursors. Most of the precursors were evaporated from open reservoirs inside the reactor, with evaporation temperatures as given in Table 4. Air-sensitive precursors were handled under argon and loaded into the reactor with the aid of N_2 purge flow. The inert gas handling was especially important for the Sr and Ba cyclopentadienyl compounds. The Sr, Ba and Bi precursors were synthesized and characterized in house at the Laboratory of Inorganic Chemistry by T. Hatanpää and T. Hänninen. The simple Ta and Ti alkoxides were commercial materials. $SrTa_2(OEt)_{10}dmae_2$ and $SrTa_2(OEt)_{10}ME_2$ were provided by Epichem.

Table 4. ALD precursor evaporation temperatures.

Precursor	Evaporation temperature (F-120)
$Bi(N(SiMe_3)_2)_3$	120–130 °C
$Ba(Me_5C_5)_2$	160 °C
$Ba(^tBu_3C_5H_2)_2$	130–140 °C
$Sr(^iPr_3C_5H_2)_2$	100–110 °C
$Sr(^tBu_3C_5H_2)2$	140–150 °C
$Ti(OMe)_4$	130–140 °C
$Ti(O^iPr)_4$	40 °C
$Ta(OEt)_5$	100°C
$SrTa_2(OEt)_{10}dmae_2$	130 °C
$SrTa_2(OEt)_{10}ME_2$	140 °C

3.2 Structural Characterization

X-ray diffraction (XRD) was used for identifying crystalline phases in the film. Three diffractometers: Philips MPD 1880, Bruker AXS D8 Advance and Panalytical XRD were used in the diffraction measurements. All instruments used Cu K_α X-rays. The Bruker AXS D8 Advance system was also used for grazing incidence XRD and X-ray reflection (XRR). Film thicknesses were measured by XRR or by fitting the optical transmittance or reflectance spectra in a wavelength range of 370 to 1100 nm.[87]

The film compositions were studied routinely by EDS, and for selected samples additional Rutherford Backscattering Spectroscopy (RBS) and Time-of-Flight Elastic

Recoil Detection Analysis (TOF-ERDA) were provided by the Accelerator Laboratory at University of Helsinki. The EDS analysis was done with two different EDS setups: an Oxford Instruments Link ISIS fitted with a Zeiss DSM 962 SEM or Oxford Instruments INCA 350 fitted with a Hitachi S4800 FESEM. The EDS data was analysed with the GMRfilm program.[88]

3.3 Film Annealing and Capacitor Structure Preparation

Film annealing treatments were done in a modified Carbolite tube furnace in O_2, N_2 or air atmosphere in a temperature range of 300–850 °C. A Nabertherm oven was used for silicon thermal oxidation with air at 1000 °C and for some of the thin film air annealing tests. An Electron Beam Evaporation (EBE) system build by Instrumentti Mattila Oy was used for the preparation of Pt, Ti and Al films for electrodes. For capacitors with indium tin oxide (ITO) bottom electrodes, top Al contacts were prepared by thermal evaporation. Two different Pt bottom electrode stacks were employed: Pt/Ti/SiO_2/Si and Pt/SiO_2/Si. The Pt/SiO_2/Si stack required a separate annealing step in air or O_2 atmosphere at 700-800 °C in order to get good Pt adhesion, but the result was a overall better capacitor. With the thinnest dielectric layers, annealing after top electrode EBE deposition gave much better results than annealing before EBE.

3.4 Electrical Characterization

Leakage current (I-V) curves were measured with a Keithley 2400 Sourcemeter or an Autolab potentiostat. The Keithley 2400 was also used for four-point probe resistance measurements of the electrode films. Capacitance measurements were done with either an HP4275 multifrequency LCR meter or an HP4284A LCR meter. A Sawyer-Tower circuit was used for studying film polarization.[89] An Agilent 33220A 20 MHz arbitrary waveform generator was used as the signal source and a National Instruments NI 5102 high-speed digitizer for recording voltage signals.

4. Atomic Layer Deposition of Binary Oxides

Each of the oxide materials of the study is discussed either in this chapter on binary oxides or in the following chapter on multicomponent oxides. An overview of the relevant literature for each material is followed by the experimental results for that material.

4.1 TiO_2

Titanium forms four different Ti(IV) dioxides: anatase, brookite, rutile and synthetic metastable TiO_2(B). The structures consist of differently interlocked TiO_6 octaedra. Numerous $TiO_{(2-x)}$ suboxide structures exist as well. TiO_2 can usually be regarded as an electrical semiconductor, though some recent reports suggest that rutile films on Ru electrodes may have good dielectric properties.[90] ALD of TiO_2 is well established.[5] In early work $TiCl_4$ was widely used as the Ti precursor. Titanium alkoxide precursors such as $Ti(O^iPr)_4$[91] and $Ti(OMe)_4$[92] are well suited for the deposition of titanate materials. The thermal decomposition limits for $Ti(O^iPr)_4$ and $Ti(OMe)_4$ are 250 °C and 350 °C, respectively.[92]

$TiCl_4$ is used in electroluminescent display production and is notanble for being stable at high temperature. The stability of earth alkaline halides $SrCl_2$ and $BaCl_2$ makes the use of $TiCl_4$ in alkaline earth metal titanate growth unlikely to succeed. The growth of Ba-Ti-O films was nevertheless attempted, at a temperature of 340 °C, with $Ba(^tBu_3Cp)_2$ as the barium precursor. The result was a highly nonuniform black Ba-Ti-O-Cl deposit. Although the use of TiI_4 was not attempted, it may warrant future attention as iodine is more readily removed from films than is chlorine. $Ti(O^iPr)_4$ and $Ti(OMe)_4$ were used in this study as the titanium sources in multicomponent oxide deposition and for TiO_2 test depositions before the work on titanate materials.

4.2 Ta_2O_5

Tantalum usually adopts oxidation state V in oxides, although Ta(IV) oxide TaO_2 with the rutile structure is also known. The crystal chemistry of Ta_2O_5 is complex, with several polymorphs observed. At low temperature, Ta_2O_5 adopts an orthorhombic

structure, but hexagonal phases can be stabilized at room temperature. Ta_2O_5 has good dielectric properties in both amorphous [93] and crystalline [94] forms, and it has excellent chemical stability. Ta_2O_5 can be grown with ALD using $Ta(OEt)_5$[95] or $TaCl_5$,[96] with H_2O, but the chloride process suffers from self-etching. Recently, TaI_5 and O_2 were used for Ta_2O_5 deposition.[97] The Ta_2O_5 process with $Ta(OEt)_5$ and H_2O [95] was used in this work for depositing capping layers on BaO and SrO. It was also used for the Ta-growth cycles in deposition of Bi-Ta-O thin films.

4.3 BaO

Barium oxide (BaO) is used as a drying agent,[98,99] as an additive in thermionic cathodes to lower the work-function,[100] in H^- ion generation for use in accelerator systems,[101] and for NO_x storage in automotive exhaust catalysts.[102] Barium oxide has a simple cubic NaCl structure. It reacts with H_2O and forms hydroxides and hydroxide hydrates $Ba(OH)_2(H_2O)_n$ (Eq. 1). In the presence of CO_2 it reacts to form $BaCO_3$ (Eq. 2).

(1) $BaO + (n+1)\ H_2O\ (g) \rightarrow Ba(OH)_2(H_2O)_n$

(2) $BaO + CO_2(g) \rightarrow BaCO_3$

The carbonate formation reaction can be reversed by annealing at temperatures above 800 °C. The use of BaO to lower the emission work function in vacuum emitter cathodes has resulted in detailed surface analysis studies being made on monolayers of BaO on tungsten surfaces. For example, Mueller et al. [100] studied reactions of H_2O and CO_2, which are the main causes of cathode poisoning, and they found that H_2O dissociates on BaO to form –OH groups. It is notable that the –OH groups seemed to be bound to W, which does not take place in the absence of Ba. The hydroxide was removed by high vacuum annealing at 327 °C, and carbonate species on surfaces exposed to CO_2 at ambient temperature were removed possible with annealing at 627 °C. Thicker BaO layers reacted with H_2O to form hydroxide.

In this work, barium oxide deposition experiments were carried out to study the absorption of H_2O in growing $Ba_xO_yH_z$ films.[VI] After capping with Al_2O_3 or Ta_2O_5 barrier films to isolate them from the environment, the deposited films were studied by

XRD. Capping was done both immediately after $Ba_xO_yH_z$ growth and after a one-hour isothermal drying period. It was found that, at 250-340 °C, absorption of H_2O into the bulk of the film significantly influences the growth chemistry. The amount of H_2O absorbed decreased both with increased H_2O purge time and with growth temperature. Films grown at 240-290 °C were amorphous or crystalline $Ba(OH)_2$, possibly with some $Ba(OH)_2(H_2O)$ present, and absorbed H_2O was not removed even after drying for one hour under N_2 flow at the growth temperature. By way of comparison, Mueller et al.[100] Mueller et al. observed dehydration of thin $Ba(OH)_2$ layers in high vacuum conditions at 327 °C. Here, although $Ba(OH)_2$ was still formed during deposition at 340 °C, it was no longer stable for extended periods of time in the ALD reactor conditions. Self-limiting growth is possible only if a constant amount of absorbed H_2O is present. The presence of self-limiting growth was not separately tested because thickness measurements of the rough and coated $Ba_xO_yH_z$ deposits were not feasible. However, with the 2000 deposition cycles used in these $Ba_xO_yH_z$ experiments, nonsaturated growth was assumed to take place on the basis of the gradual release of the H_2O absorbed during the water pulses.

4.4 SrO

SrO has a similar structure to BaO, but it is slightly less reactive with H_2O than BaO is. The tendency to form $M(OH)_2$ decreases in the series, Ba > Sr > Ca. ALD growth of crystalline CaO at 300 °C was reported by Kukli et al.[103] using fairly short H_2O purge times. Interest in SrO thin films has dramatically increased owing to the use of these films as an interface layer for epitaxial growth of $SrTiO_3$ on silicon. Heteroepitaxy of SrO on silicon was first demonstrated by Kado and Arita.[104] Later, SrO monolayers on a Sr silicide interface were demonstrated to yield a good heteroepitaxial interface to $SrTiO_3$. [105, 106] High vacuum techniques like MBE and PLD have so far been required to make good epitaxial SrO layers.

In this work, deposition of uniform SrO films proved significantly easier than BaO growth. At 300 °C, SrO films were obtained on Si substrates with both $Sr(^tBu_3Cp)_2$ and $Sr(^iPr_3Cp)_2$ with H_2O as the oxygen source. A 120–160 nm thick Ta_2O_5 barrier layer was deposited by the $Ta(OEt)_5/H_2O$ process to protect against reactions with air moisture and CO_2. As a precaution, the capping of SrO was started with 20 separate $Ta(OEt)_5$ exposures to limit the exposure of the underlying SrO to the H_2O pulses used

in subsequent Ta_2O_5 growth. The growth rate with $Sr(^tBu_3C_5H_2)_2$ at 300 °C was 0.28 Å/cycle. With $Sr(^iPr_3C_5H_2)_2$ the growth rate was 0.42 Å/cycle with a 0.6 s pulse length. The growth rate did not markedly slow when the H_2O purge time was increased from 2 to 5 s. Doubling the $Sr(^iPr_3C_5H_2)_2$ pulse length almost doubled the growth rate, to 0.75 Å/cycle, with an associated increase in thickness profile. Evidently, $Sr(^iPr_3C_5H_2)_2$ and H_2O do not provide fully self-limiting growth of binary SrO at 300 °C. SrO films were strongly crystalline with pronounced (111) orientation (Figure 12), as shown by the clear XRD rocking curve maximum (Figure 12 inset).

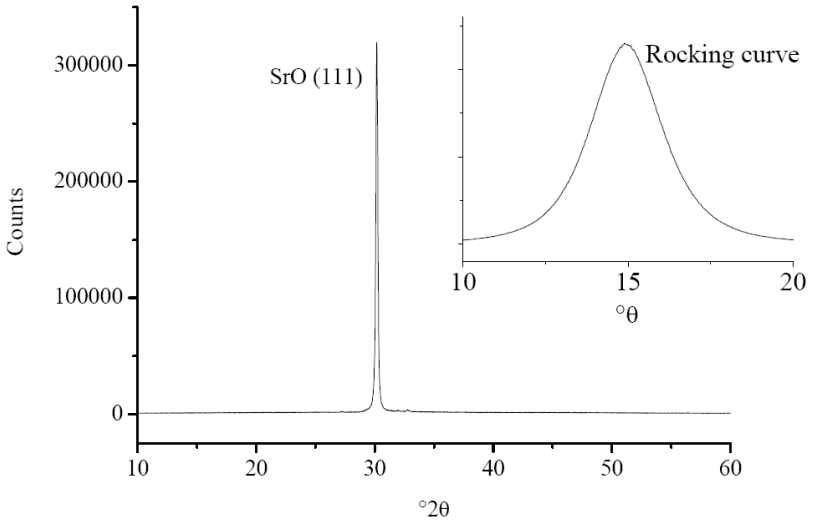

Figure 12. XRD pattern of a Ta_2O_5/SrO/Si stack deposited at 300 °C, with rocking curve of the SrO (111) peak shown in the inset. The thickness of the SrO layer is 83 nm.

4.5 Bi_2O_3

Bismuth forms several Bi(III) oxides of which the low temperature monoclinic form is the most common. The high temperature cubic delta phase of Bi_2O_3 is stabilized in thin film form, and it has the highest known oxygen ion mobility, which may be of use in solid oxide fuel cells.[107] Bismuth also forms sub-oxides such as $Bi_2O_{2.33}$ in which lower bismuth oxidation states are present.[108] Bi_2O_3 is an important additive in oxidation catalysts.[109, 110] Bismuth oxides are highly reactive in the solid state and form multicomponent oxide mixtures with most other metal oxides. The fast/ready diffusion of bismuth allows it to act beneficially as a flux for forming complex structures, but it can also lead to unwanted interface reactions.

In this work, bismuth oxide films were deposited with alternating $Bi(N(SiMe_3)_2)_3$ and H_2O pulses at 190-200 °C, which is close to the thermal stability limit of $Bi(N(SiMe_3)_2)_3$.[IV,V] Growth rates of amorphous BiO_x films in the range of 0.08-0.20 Å/cycle were observed, but the rate varied from experiment to experiment. One possible explanation for the variation is partial reduction of bismuth during the $Bi(N(SiMe_3)_2)_3$ pulses, making the growth sensitive to small variations in the precursor dose. Separate exposure tests were done with the protonated ligand $H\text{-}N(SiMe_3)_2)_3$, a likely byproduct, but no reduction of bismuth oxide was observed. If excess ligand is present in the precursor it could cause variation in the growth by blocking adsorption sites.

BiO_x films grown on silicon and on Al_2O_3 coated silicon were useful for studying the reactivity of bismuth oxide films with substrate materials. When BiO_x films grown on Si were annealed in air, bismuth silicate Bi_2SiO_5 began to form at 500 °C, and at 750 °C the bismuth oxide had quantitatively reacted with silicon (Figure 13). Aluminium bismuth oxide $Al_4Bi_2O_9$ was quantitatively formed when BiO_x films on buffer Al_2O_3 layers were annealed at 750 °C.

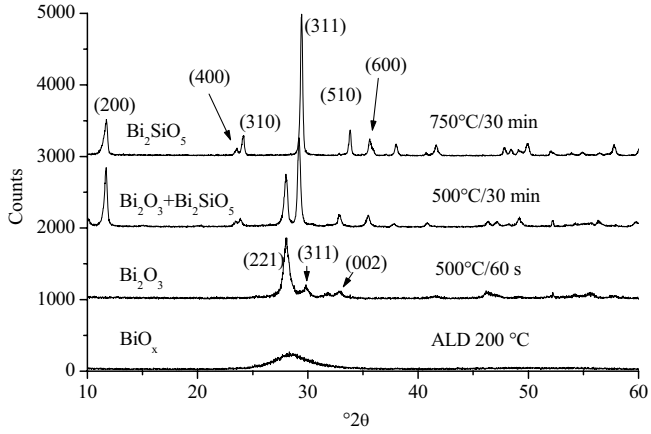

Figure 13. GIXRD measurement of as-deposited and air-annealed BiO_x films. An incident angle of 1° was used in the measurements.

5. Atomic Layer Deposition of Multicomponent Oxides

5.1 $SrTiO_3$

$SrTiO_3$ is a widely studied material for to several reasons. It has high tunable permittivity at low temperature,[111] and good microwave dielectric properties, [112] it can be used in combination with superconducting materials,[113] and in the future it might be useful in semiconductor applications owing to its high relative permittivity (about 330 for bulk single crystals at room temperature).[114] Recently, Haeni and coworkers[58] demonstrated induced room temperature ferroelectricity in strained $SrTiO_3$ films.

Deposition of $SrTiO_3$ thin films has been studied extensively by other deposition methods than ALD, including sputtering, [115] MOCVD,[116] MBE,[117] PLD[118] and sol-gel.[119] Making low leakage MIM capacitors with $SrTiO_3$ thin film dielectrics generally requires high work function electrodes.[120] $SrTiO_3$ has also been considered for use as an epitaxially grown gate dielectric in MOSFETs,[105, 106] but getting well-perfoming devices requires careful interface engineering.[121] The permittivity of $SrTiO_3$, similar to that of other perovskite dielectrics, decreases with decreasing film thickness owing to what is often called an interface dead layer effect.[122] The thickness of the dead layer and the causes for its formation are still not well understood, and may depend on multiple factors such as mechanical strain, contaminants, roughness of the interfaces and the microstructure of both the dielectric and the electrode.[123]

In this work, growth of $SrTiO_3$ was studied with two different sets of precursors: $Sr(^iPr_3C_5H_2)_2$, $Ti(O^iPr)_4$ and H_2O[I, II] and $Sr(^tBu_3C_5H_2)_2$, $Ti(OMe)_4$ and H_2O. When $Sr(^iPr_3C_5H_2)_2$ was used as the Sr source, experiments were done in the temperature range of 250–325 °C, the lowest temperature being close to ideal ALD conditions.[II] The growth with $Ti(O^iPr)_4$ has CVD component at the upper end of the growth temperature range, but temperatures in the range of 300-325 °C were still studied in more detail as the as-grown films turned out to be well crystallized at 325 °C even on amorphous substrates. This is a remarkably low crystallization temperature for $SrTiO_3$ thin films deposited by gas-phase methods.

At 250 °C, highly uniform films were obtained with growth rates of approximately 0.5 Å/cycle. A roughly 0.1 Å/s increase in the growth rate was observed with increasing $Sr(^iPr_3C_5H_2)_2$ pulse length. Previously thought to be due to Sr precursor

decomposition, it is likely better explained by insufficient H_2O purge time resulting in $Sr(OH)_2$ formation. Ihanus et al. [124] used $Sr(^iPr_3C_5H_2)_2$ for SrS growth and found the thermal decomposition to begin at 380 °C, further pointing to other causes than decomposition for the growth rate increase in the water process. In scale-up experiments, Sr-Ti-O films of uniform composition and thickness were grown on 30x40 cm glass substrates in a F-450 pilot reactor at 250 °C,[125] but large area growth was not possible above this temperature, possibly due to the influence of hydroxide formation and the beginning of thermal decomposition of $Ti(O^iPr)_4$. Films deposited at 250 °C were mostly amorphous.(I,II)

When films were grown above the thermal decomposition limit of $Ti(O^iPr)_4$ they began to crystallize during the growth after about 50 nm onset thickness, first in a random orientation and then in a preferred (100) orientation.[II,126] High water doses, possibly leading to excess $Sr(OH)_2$, were found to enhance crystallization, and in some cases crystalline substrates aided the crystallization of the films, shown as amorphous Al_2O_3 vs. crystalline Pt in Figure 14. As an extreme case, deposition of $SrTiO_3$ on an MBE-grown seed layer at 325 °C led to direct epitaxy without any clear interface between the MBE and ALD films (Figure 15).[126]

An improved process with $Sr(^tBu_3C_5H_2)_2$ and the thermally more stable $Ti(OMe)_4$ precursor was used to grow $SrTiO_3$ films at 300 °C. The earlier approach of high water doses was not attempted in order to avoid difficulties in purging. This process has been adapted by ASM Microchemistry for deposition on up to 300 mm wafers. Growth with 1:1 Sr:Ti cycle ratio (Figure 16) results in self-limiting growth rate of 0.40 Å/cycle and a Sr/(Sr+Ti) ratio of 0.30. In this case each Sr-O cycle is preceded by a Ti-O cycle, and the growing surface has, on the average, excess titanium. When a second consecutive Sr-O cycle is applied in a 2:1 Sr:Ti cycle ratio, reaching saturation is no longer as easy, and an increase in the growth rate as compared with the 1:1 cycle ratio is observed, as shown in Figure 17. The average surface composition during a Sr-O growth cycle clearly influences the growth behaviour. Further development will focus on controlling the surface composition by seeking alternative titanium sources with sufficient thermal stability and larger ligands, i.e., lower growth rate relative to Sr so that the number of consecutive Sr-O reactions can be reduced.

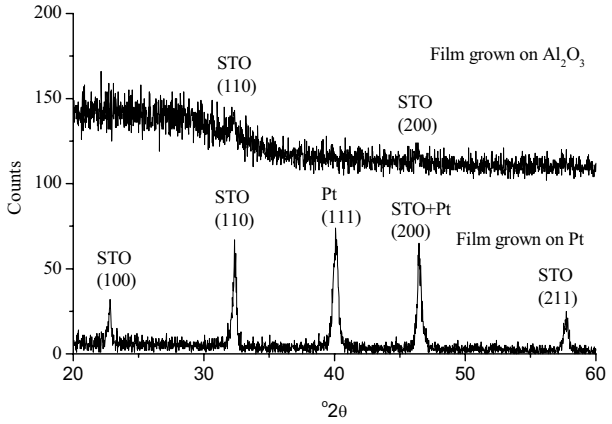

Figure 14. GIXRD pattern of an as-deposited 140 nm $SrTiO_3$ film, grown in the same ALD experiment on Al_2O_3 coated glass and on a Pt/Ti/SiO_2/Si substrate. The $SrTiO_3$ films were deposited at 275 °C with $Sr(^iPr_3C_5H_2)_2$, $Ti(O^iPr)_4$ and H_2O.

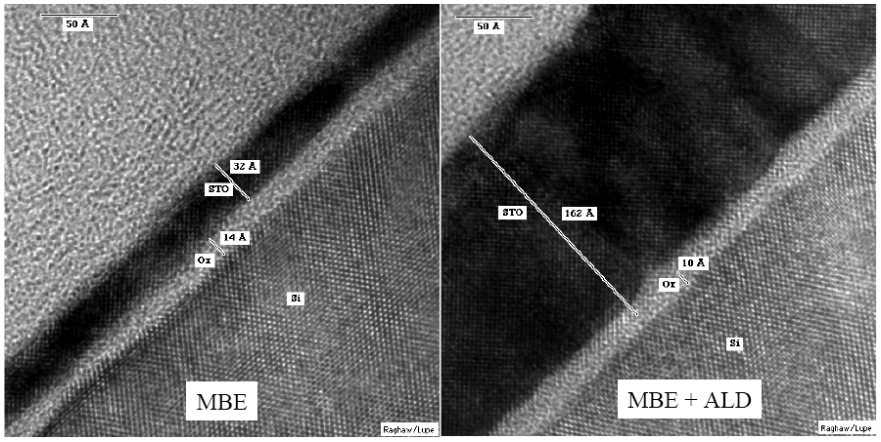

Figure 15. HRTEM images showing the influence of an epitaxial MBE seed layer on ALD growth. A SiO_2 layer whichs forms during processing is seen between Si and the epitaxial $SrTiO_3$.

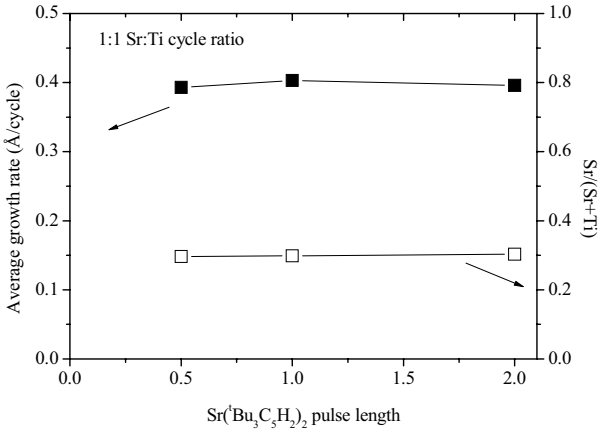

Figure 16. Saturation of growth rate and composition for Sr-Ti-O grown with a 1:1 cycle ratio at 300 °C with $Sr(^tBu_3C_5H_2)_2$, $Ti(OMe)_4$ and H_2O as the precursors.

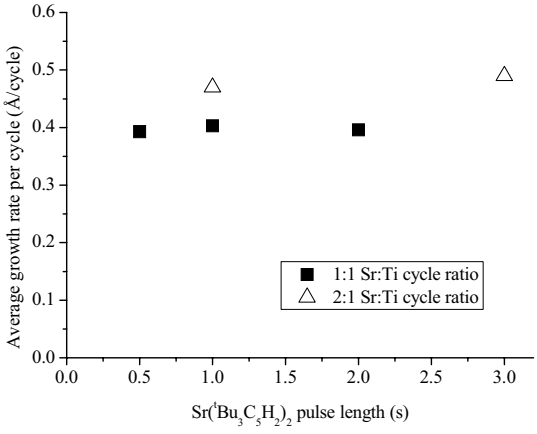

Figure 17. Growth rate on Si substrates at 300 °C as a function of the $Sr(^tBu_3C_5H_2)_2$ pulse length at 1:1 and 2:1 Sr:Ti ratios.

The dielectric properties of the $SrTiO_3$ films were studied with MIM capacitors fabricated with ITO/Al and Pt/Pt electrode configurations. In the initial studies, Pt films were prepared on glass with Ti adhesion layers, and in the later experiments Pt electrodes were prepared on thermally oxidized silicon substrates without an adhesion layer. As expected from the literature,[120] leakage was lower with Pt electrodes (Figure

18). A 490 nm film grown on Pt at 325 °C from $Sr(^{i}Pr_3C_5H_2)_2$, $Ti(O^{i}Pr)_4$ and H_2O had a permittivity of 130 after annealing in air at 500 °C (Figure 19).

MIM capacitors were also prepared by depositing sub-100 nm $SrTiO_3$ films with $Sr(^{t}Bu_3C_5H_2)_2$, $Ti(OMe)_4$ and H_2O on $Pt/SiO_2/Si$ substrates at 300 °C. A 49 nm film annealed in O_2 at 750 °C had a permittivity of 90 at 1 V, resulting in an EOT of 2.2 nm. Figure 20 shows the EOT and dielectric loss of the 49 nm thick $SrTiO_3$ film with Pt electrodesas as a function of bias voltage. An EOT–V plot is useful for evaluating thin MIM capacitors with nonlinear dielectrics such as $SrTiO_3$ because a single EOT value is not well suited for describing capacitor performance. The leakage currentsof $SrTiO_3$ capacitors with dielectric thickness < 50 nm were fairly high compared to $BaTiO_3$ and BST films of similar thickness, above $1.0 \bullet 10^{-5}$ A/cm^2 at 1 V. For comparison, permittivity values reported by Kiyotoshi et al. [127] for ultra-thin epitaxial $SrTiO_3$ films prepared on Nb:$SrTiO_3$ were 160 and above for films thicker than 20 nm, but a decrease of the permittivity to 87 was measured for a 10.4 nm film, resulting in an EOT of 0.48 nm.

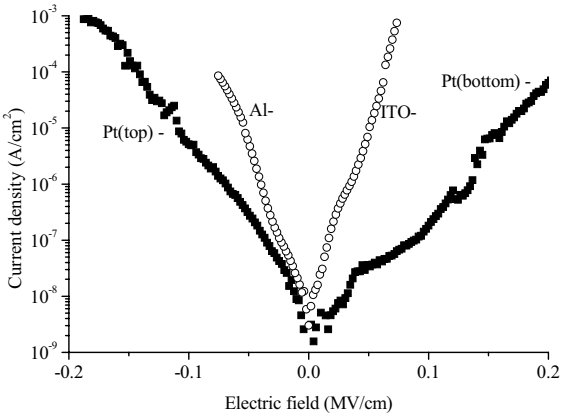

Figure 18. Comparison of the leakage current density in $SrTiO_3$ prepared with $Sr(^{i}Pr_3C_5H_2)_2$, $Ti(O^{i}Pr)_4$ and H_2O with either ITO/Al or Pt/Pt electrodes.

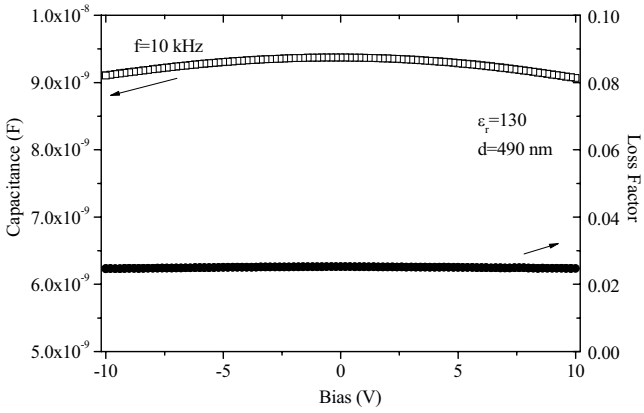

Figure 19. Capacitance and loss versus voltage of a $SrTiO_3$ capacitor annealed at 500 °C, showing the typical nonlinear polarization observed in paraelectric $MTiO_3$ (M= Ba, Sr) materials.

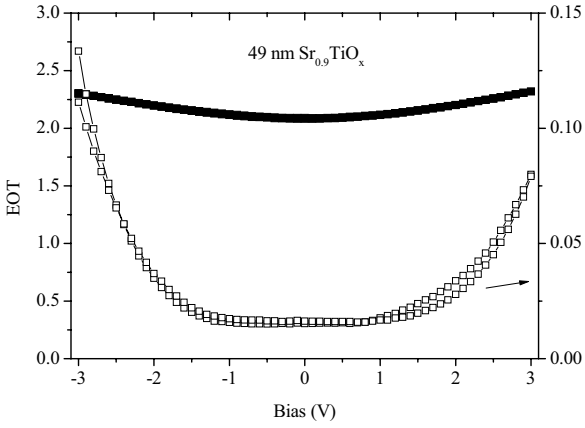

Figure 20. EOT and dielectric loss of a Pt/49 nm $SrTiO_3$/Pt capacitor.

5.2 $BaTiO_3$

The high dielectric permittivity, and later the ferroelectricity of $BaTiO_3$, was discovered during World War II, and was first used for communications, underwater transducers and capacitors.[128,129] Since then, $BaTiO_3$ has enjoyed wide use in ceramic capacitors and positive temperature coefficient resistor (PTCR) elements.[130,131] The permittivity of crystalline $BaTiO_3$ can be as much as several thousand in ceramics and thick single

crystals, but is generally much lower in films less than 1 μm thick. In thin films, the ferroelectricity of $BaTiO_3$ is often reduced or fully suppressed by extrinsic effects such as stress.[132] Recent work has shown that $BaTiO_3$ can remain ferroelectric at film thicknesses below 5 nm if favourable substrate materials are used.[133] The ferroelectric remanent polarization of $BaTiO_3$ can even be enhanced from the bulk value of 26 $\mu C/cm^2$ up to 70 $\mu C/cm^2$ by using substrate materials that cause uniform stress in the film.[134] $BaTiO_3$ thin films have been prepared by sputtering,[135] PLD,[136] CSD methods such as sol-gel and MOD,[137] and MOCVD.[138] PLD is currently the most important method for preparing epitaxial structures for device physics studies. $BaTiO_3$ thin films can also be used as dielectrics in an amorphous form, bringing the advantage of a much lower process temperature that is required for crystalline $BaTiO_3$ films.[139, 140, VI]

In this work Ba-Ti-O films were deposited using Ba cyclopentadienyl precursors and titanium alkoxides. $Ba(Me_5C_5H_2)_2$ was the first barium source to be tested,[I] but growth of reasonably uniform films was limited to 275 °C. Hatanpää et al.[9] screened a wide range of cyclopentadienyl compounds and found that $Ba(^tBu_3C_5H_2)_2$ was the most stable. Crystalline $BaTiO_3$ films were grown at 350 °C with this Ba precursor and $Ti(O^iPr)_4$ as the titanium precursor. The high growth rates up to 1.0 Å/cycle in this preliminary study were most likely due to a surface hydroxide contribution to the film growth and thermal decomposition of $Ti(O^iPr)_4$.

A strong influence of water purging time was found in growth at 250 °C with $Ba(^tBu_3Cp)_2$, $Ti(O^iPr)_4$ and H_2O. Growth rates at different Ba:Ti cycle ratios are shown in Figure 21, and growth rates as a function of the water purging time with two sets of metal precursor pulse times are set out in Figure 22. Even though fairly uniform films could be grown with fixed precursor pulse lengths and sufficiently long H_2O purge times, the required H_2O purge time was seen to increase with longer $Ba(^tBu_3C_5H_2)_2$ pulses, resulting in nearly doubled growth rates in the 1–3 second pulse and purge timescale often used in practical ALD. Low temperature ALD of barium-containing oxides with H_2O can thus be both difficult and time consuming. The situation was improved considerably in higher temperature processing with $Ti(OMe)_4$ as the titanium source, and self-limiting conditions were found.[VI] In general it can be assumed that Ba-Ti-O growth with H_2O as the oxygen source becomes easier with lower Ba content in

the film and with as high as possible process temperature, as long as precursor self-decomposition is avoided.

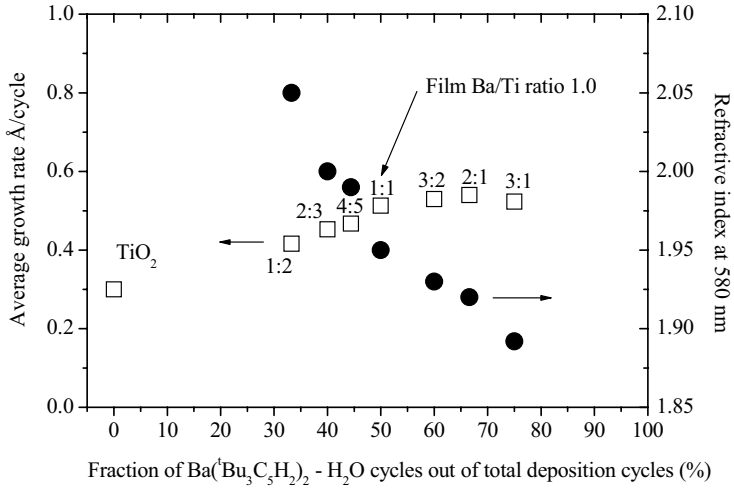

Figure 21. Growth rate and refractive index of Ba-Ti-O films prepared with different Ba:Ti cycle ratios.

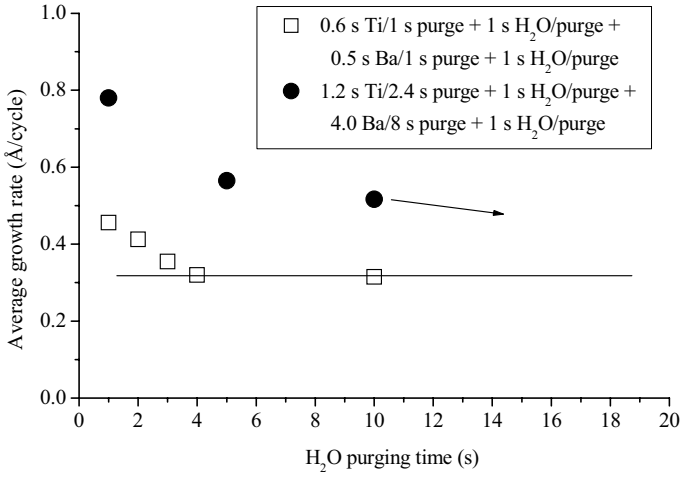

Figure 22. The growth rate of Ba-Ti-O films at 240 °C as a function of the H_2O purge time.

MIM capacitors with a permittivity of 280 at 1 V were obtained from the low temperature grown 140 nm thick $BaTiO_3$ films after annealing at 800 °C (Figure 23). It is notable that an EOT below 2 nm can be reached with films as thick as 140 nm within the ± 1.6 V bias range. With thinner films prepared at 340 °C, slightly improved EOT of 1.8 nm at 1 V bias was achieved.[VI] Further improvements in $BaTiO_3$ capacitors will require fine-tuning of the dielectric composition, preparation of high quality electrode interfaces and refined annealing methods, possibly rapid thermal annealing (RTA).

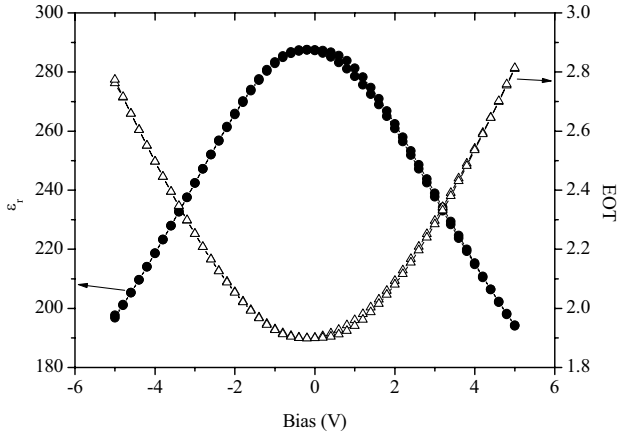

Figure 23. Permittivity and EOT of a 140 nm $BaTiO_3$ film as a function of bias voltage.

5.3 $Ba_{(1-x)}Sr_xTiO_3$

$Ba_{(1-x)}Sr_xTiO_3$ (BST) is a full solid solution of $BaTiO_3$ and $SrTiO_3$ in which a change in the Ba/Sr ratio strongly influences the dielectric properties of the material. In bulk ceramics, the Ba/Sr ratio can be used to control the ferroelectric to paraelectric transition and the associated permittivity maximum of $Ba_{(1-x)}Sr_xTiO_3$.[128] Much research effort has focused on the preparation of BST thin films for DRAM capacitors, [141, 142, 143] but so far BST films have not been adopted into DRAM production. Tunable capacitors for microwave devices are a promising application for BST.[144] The main integration issues are the same as for $BaTiO_3$ and other ferroelectric materials: the need for high work function electrodes such as Pt and a high thermal budget.

BST thin films have been prepared by sputtering[145, 146] and MOCVD [147, 148] which are the most viable methods for future DRAM capacitors, and by sol-gel [149] and PLD [150] methods, which are often used in materials research and non-IC applications. A general observation is that the film permittivity decreases along with film thickness.[151] As with $BaTiO_3$, residual stress in the capacitor film stack influences the dielectric properties.[152]

In this work, initial BST deposition experiments were made by combining $BaTiO_3$ and $SrTiO_3$ processes. With a total of four separate precursors for Ba, Sr, Ti and O, ALD of BST is highly complex as compared with binary oxide growth. Nevertheless, even a simple 1:1:1 Ti:Ba:Sr growth cycle sequence used in deposition tests at 300°C with $Ti(OMe)_4$, $Ba(^tBu_3Cp)_2$ and $Sr(^tBu_3Cp)_2$ as the metal sources yielded high charge density $Ba_{(1-x)}Sr_xTiO_3$ capacitors. The 1:1:1 cycle ratio was chosen as a starting point because 2:1 Ba:Ti and Sr:Ti cycle ratios were seen to result in close to stoichiometric $SrTiO_3$ and $BaTiO_3$ films, owing to the small size of the –OMe ligand in titanium methoxide. The cycle order Ti–Ba–Sr was chosen on the basis of experience with $BaTiO_3$. Thus, the most H_2O sensitive component Ba was deposited right after Ti-OH groups were created during the preceding $Ti(OMe)_4$ – H_2O cycle. As the Ba and Sr precursors had the same ligand they were introduced into the film in more or less equal amount. In the initial experiments the Ba/Sr ratio in the film was clearly influenced by the precursor dose, as shown in Table 5. It is noteworthy that increased Ba content slightly lowered the amount of Sr incorporated during the next cycle, possibly due to the reduced availability of Ti-OH groups during the Sr-O deposition cycle. Separating the Ba and Sr cycles from each other might prove beneficial in the future. This could be possible if a non-halide Ti precursor with larger ligands was found.

Table 5. EDS results for a sample set prepared with 1:1:1 Ti:Ba:Sr or 2:1 Sr:Ti cycle ratios. Fixed pulse lengths of 1.5 s, 1.0 s and 1.0 s were used for Ba, Sr and Ti, respectively.

	Ba atom %	Sr atom %	Ti atom %	Ba/Sr	(Ba+Sr)/Ti	Sr/Ti
170 nm BST film, 1:1:1 cycle ratio a)	10.8	8.3	20.6	1.30	0.93	0.40
170 nm BST film, 1:1:1 cycle ratio b)	12.0	7.9	20.1	1.52	0.99	0.39
150 nm $SrTiO_3$ film, 2:1 cycle ratio	0	17.4	21.8	0	0.80	0.80

a) $Ba(^tBu_3Cp)_2$ evaporation temperature of 130-140 °C, b) evaporation temperature of 145-155 °C

BST MIM capacitors were prepared by depositing films at 300 °C on Pt substrates, and afterwards fabricating Pt top electrodes by EBE. Crystallization annealings were carried out in either N_2 or O_2 atmosphere, or both of them separately. For films crystallized in N_2, an additional anneal in O_2 at 600 °C reduced the leakage current density, as shown in Figure 24. The annealing time that yielded intact capacitors was shorter with decreasing film thickness. Whereas 30 min at 750 °C was good for 54 nm capacitors, the same anneal time resulted in a short circuit for 35 nm films. Intact capacitors with 35 nm films were fabricated with a 2 min anneal at 750 °C. It seems that the annealing treatment should be separately optimized each time a change is made to the electrode surface, the BST dielectric composition or the BST dielectric thickness. As shown in Figure 25, the relative permittivity of BST films decreased from 240 for a 170 nm film to 135 for a 35 nm film. The best EOT at 1 V bias was 1.08 nm for a 35 nm BST film (Figure 26), with leakage current density of $1 \cdot 10^{-5}$ A/cm^2 at the same voltage (Figure 27).

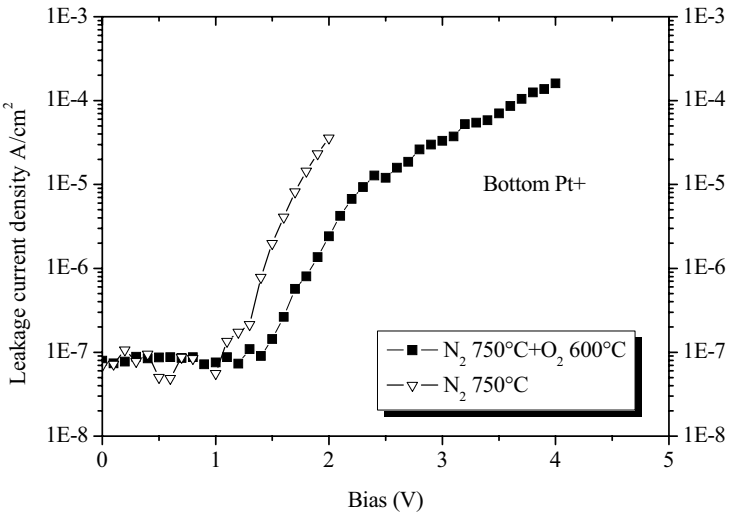

Figure 24. Leakage current density for a 54 nm BST film crystallized at 750 °C in N_2 with and without an additional O_2 anneal at 600 °C.

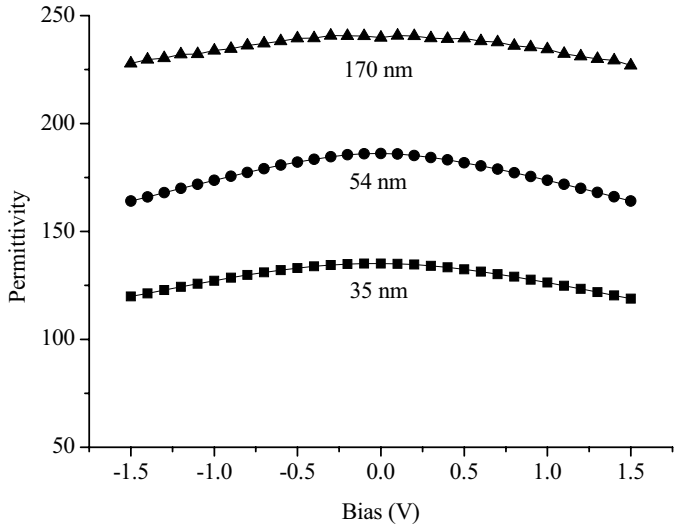

Figure 25. BST film permittivity as a function of the bias voltage for three film thicknesses.

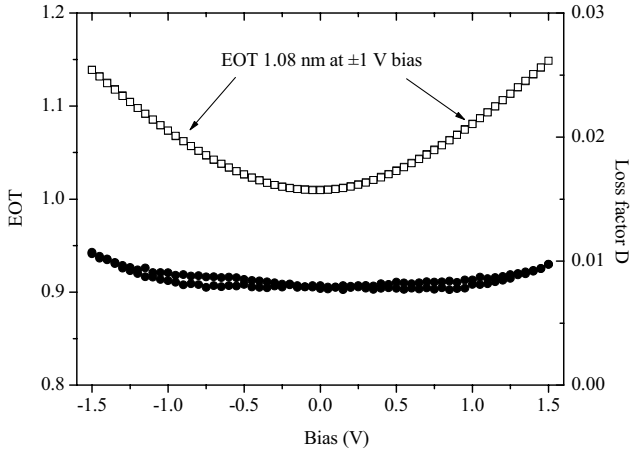

Figure 26. EOT and dielectric loss as a function of bias voltage of a 35 nm Pt/BST/Pt capacitor.

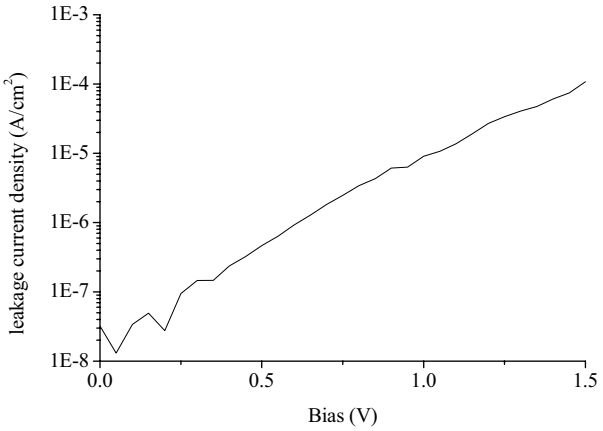

Figure 27. Leakage current density of a 35 nm Pt/BST/Pt capacitor with current injection from the top electrode surface.

5.4 $SrTa_2O_6$ and $BiTaO_4$

Strontium tantalates such as $SrTa_2O_6$ form complicated structures with perovskite-like building blocks. A metastable cation-deficient simple perovskite $Sr_xTa_xO_3$ ($x \sim 0.85$) phase has also been found in thin films.[153] Preparation of $SrTa_2O_6$ thin films became interesting as a part of the development of processes for $SrBi_2Ta_2O_9$.[154, III, IV] More recently there has been interest in using $SrTa_2O_6$ as such, in view of the reasonably high permittivities of about 40 that have been achieved with amorphous Sr-Ta-O films.[155-158] Bi-Ta-O, for its part, is a good dielectric material both in thin film [157, 158] and in ceramic form.[159] Thin $BiTaO_4$ layers have also been used as interface dielectrics for SBT films,[160] and the solid solution $BiTa_{(1-x)}Nb_xO_5$ has photocatalytic properties.[161]

In this work, bimetallic precursors $SrTa_2(OEt)_{10}ME_2$ (ME = methoxyethoxide) and $SrTa_2(OEt)_{10}dmae_2$ (dmae = dimethylaminoethoxide) were used to prepare $SrTa_2O_6$.[III] Well-controlled growth of $SrTa_2O_6$ was achieved with $SrTa_2(OEt)_{10}dmae_2$ in the temperature range of 200-300 °C, though some deviation from the molecular Sr:Ta ratio was observed. This may have been due to surface dissociation or disproportionation. Although the $SrTa_2(OEt)_{10}dmae_2$ precursor is not necessarily the best choice for preparing $SrBi_2Ta_2O_9$, as the Sr/Ta ratio cannot be freely adjusted, the possibility of introducing two cations in a single reaction cycle has the potential to

greatly simplify multicomponent oxide film deposition. It should be noted that, since Sr is present in the film, the use of longer H_2O purge times might result in better stand-alone $SrTa_2O_6$ dielectrics.

Bismuth tantalate films were grown with $Bi(N(SiMe_3)_2)_3$, $Ta(OEt)_5$ and H_2O as the precursors.[IV] Thermal decomposition of $Bi(N(SiMe_3)_2)_3$ limited the experiments to 190 °C. The problems observed in BiO_x growth were eliminated with closely mixed $Ta(OEt)_5$ – H_2O cycles, and the result was reproducible and well saturated growth.

5.5 $SrBi_2Ta_2O_9$

Layered perovskite $SrBi_2Ta_2O_9$ (SBT) is one of the two materials currently used in commercial FRAM, the other being PZT.[162] The key advantages of SBT are that reliable devices can be processed on Pt electrodes [163] and that it has a low coercive field even in ultra-thin films.[164] The main disadvantage of SBT is the high process temperatures, 700-850 °C in oxygen atmosphere, required to obtain the Aurivillius phase. This makes SBT integration more complex.[165, 166] Unwanted pyrochlore and fluorite-type SBT is often encountered in thin films processed at low temperature or with Bi-deficient compositions.[67,68] Also, as the ferroelectric polarization is only in the a-b plane direction,[62] the ferroelectric properties are highly sensitive to the crystallographic orientation and texture of the film.[167, 168]

The most successful approaches for large-area SBT deposition have been solution methods [67,169,170] and MOCVD,[171-173] which in favourable cases lead to small randomly oriented SBT grains after RTA. For academic studies, epitaxial as-deposited ferroelectric SBT structures have been prepared by PLD.[167, 174] Sputtering can be used for SBT deposition too, but the film composition is sensitive to processing parameters such as the chamber pressure and target-sample distance.[175] Common to all methods that require crystallization annealing is the risk bismuth diffusion and degrading of the electrode films. This effect is most easily minimized by RTA.[176]

In this work SBT films were deposited by the process for growing Bi-Ta-O but with $Ta(OEt)_5$ replaced by $SrTa_2(OEt)_{10}dmae_2$. Saturated growth of Sr-Bi-Ta-O films was achieved at a 2:1 Bi/(Sr+Ta) cycle ratio, resulting in a $Sr_{0.8}Bi_{2.1}Ta_2O_x$ stoichiometry.[IV] The films deposited at low temperature contained large amounts of hydrogen, a result that is partly explained if the solid is a mixture of $Sr(OH)_2$, Ta_2O_5, and Bi_2O_3.

The as-deposited films were apparently uniform, but during furnace annealing film crystallization took place in a highly non-uniform fashion across the substrate, with high roughness regions, porosity and delamination observed, especially if Pt coated substrates were used. SBT has a strong tendency to form elongated grains, and this is the main reason for the common use of RTA methods. RTA gives sufficient energy for crystallization but limits the time available for grain growth. Causes for the variation in the crystallization behaviour may include spatial variation of the Sr:Bi:Ta composition and of the impurities. When the H_2O purge time was increased from 2 to 5 seconds, the roughening of the film during crystallization was reduced and fabrication of test capacitor structures became possible.

Obtaining Aurivillius-type SBT by annealing ALD films on silicon required temperatures in the range of 750-850 °C in a tube furnace. These high temperatures made preparation of intact Pt/SBT/Pt capacitors difficult, with all experiments with dielectric layers <100 nm resulting in short circuits. Intact capacitors were succesfully prepared with 190 nm SBT layers by first depositing a 30 nm seed layer, which was crystallized at 800 °C and then depositing a second 160 nm layer, which in turn was crystallized at 800 °C. The pyrochlore phase was also apparent in the GIXRD pattern, shown in Figure 28.

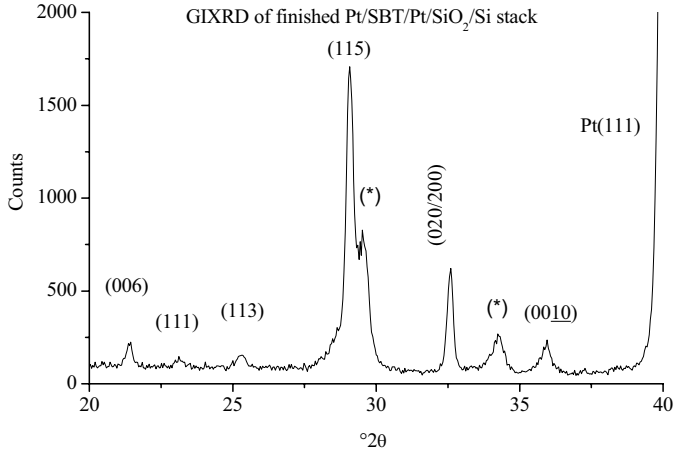

Figure 28. GIXRD pattern of SBT film crystallized in two steps on a $Pt/SiO_2/Si$ substrate. The secondary pyrochlore phase is denoted by (*).

The peaks in the figure are indexed through reference to the table of Lee et al.[177] The use of seed layers was observed by Jung et al. [178] to improve the phase purity of SBT films prepared by the sol-gel method. The C-V and Q-V plots of the capacitor with 190 nm SBT are shown in Figures 29 and 30. The presence of the secondary phase likely explains the relatively low permittivity and remanent polarization of 70 and 0.75 $\mu C/cm^2$, respectively. The leakage current of the ferroelectric capacitor was below $1.5 \cdot 10^{-7}$ A/cm^2 in a ±4 V sweep voltage range, showing that the hysteresis loop measured with a 1 kHz (Figure 30) can be regarded as true ferroelectric hysteresis.

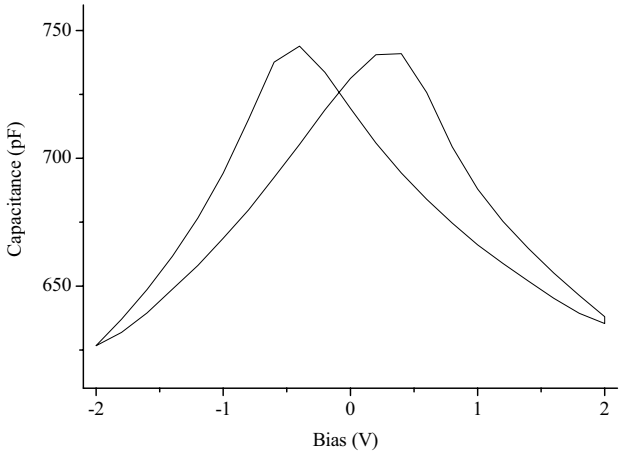

Figure 29. C-V measurement of the Pt/SBT/Pt capacitor shown in Figure 28. The permittivity of the film at zero bias voltage was 70.

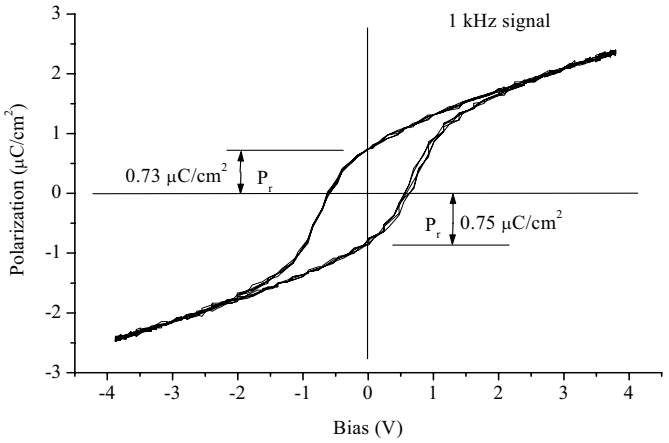

Figure 30. Sawyer-Tower Q-V loop of a Pt/SBT/Pt capacitor structure.

5.6 $Bi_4Ti_3O_{12}$

Layered perovskite bismuth titanate $Bi_4Ti_3O_{12}$ is a promising candidate for use in electro-optic switches [179,180] and in high-temperature piezoelectric applications such as pressure sensors.[181] It has also been considered for use in ferroelectric field-effect transistor gate stacks,[182,183] with many studies focusing on lanthanide-modified films.[184] The electrical properties of undoped $Bi_4Ti_3O_{12}$ are sensitive to oxygen vacancies and thus annealing treatments should be done in oxygen-rich atmospheres.[185,186,V] The addition of lanthanide elements [65] and co-dopants serves to reduce the oxygen vacancy concentration and immobilize the remaining oxygen vacancies.[187,188]

Bismuth titanate thin films have been prepared by most thin film deposition methods including PLD,[189] sputtering,[190] laser MBE,[191] MOCVD,[192,193] CVD[194] and sol-gel.[195] Generally, c-axis oriented films have remanent polarizations up to 4 $\mu C/cm^2$, provided that they are thick enough.[193] Much higher polarizations are observed for non-c-axis and randomly oriented films.[190,192]

In this work bismuth titanate films were grown by mixing $Bi(N(SiMe_3)_2)_3 - H_2O$ growth cycles with $Ti(OMe)_4 - H_2O$ cycles at 190 °C. With a 1:1 Bi:Ti cycle ratio, films were very smooth and homogeneous, but as more consecutive $Bi(N(SiMe_3)_2)_3 - H_2O$ cycles were introduced, the surface morphology of the films began to change, with

nanoscale mounds forming on the surface. This was attributed to partial reduction of bismuth during the $Bi(N(SiMe_3)_2)_3$ pulse. The formation of nanoscale features was also observed in BiO_x films.[V] By way of comparison, Schuisky et al.[11] observed strong reduction to metallic bismuth when $Bi(Ph)_3$ was used as the bismuth source for growth of Bi-Ti-O films with H_2O as the oxygen source.

Bi-Ti-O films were easy to crystallize in the temperature range 500–750 °C. At 750 °C the grain growth is highly aggressive, as shown in Figure 31 for a 51 nm thick film with a composition of $Bi_{1.40}TiO_x$. When lower temperatures 550-650 °C were used for the crystallization, randomly oriented $Bi_4Ti_3O_{12}$ films were prepared. Ferroelectric films with remanent polarizations up to 0.5 $\mu C/cm^2$ were prepared on $Pt/SiO_2/Si$-substrates by annealing initially at 500 °C and finally at 600 °C. Similar to the case with thin alkaline earth metal titanate films, it was difficult to prepare intact devices if the top electrode film was not deposited before crystallization.

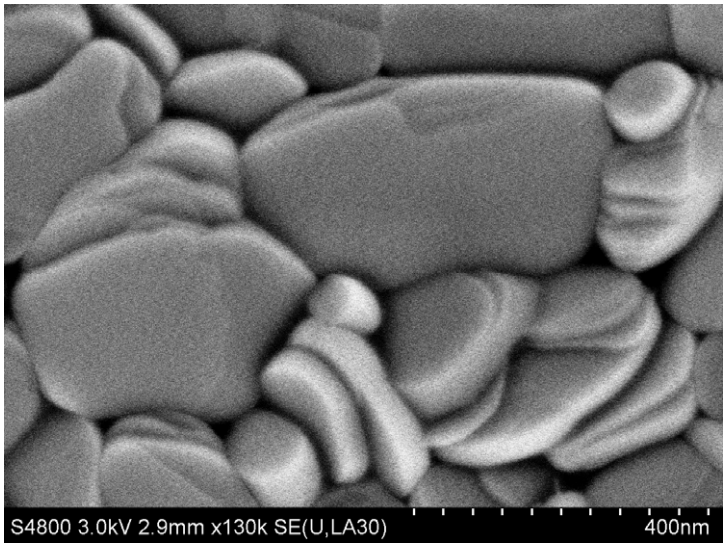

Figure 31. $Bi_4Ti_3O_{12}$ grains formed by crystallization of an amorphous 51 nm $Bi_{1.40}TiO_x$ film at 750 °C. Lateral grain dimensions up to 10 times the film thickness can be seen.

6. Conclusions

There is great need in the IC industry for improved metal–insulator–metal stacks that simultanously achieve high charge densities, low leakage, and as low overall thermal budget as possible. The development of methods to prepare the required thin film materials uniform and conformal on large area surfaces is an urgent requirement. Improvements in multicomponent oxide dielectric fabrication could well be the enabling technology not just for future generations of memory devices but also for more specialized applications such as integrated RF circuits.

The primary goal of this study was to develop self-limiting ALD processes for multicomponent oxides containing two or more metal cations, especially ones potentially useful as dielectric and ferroelectric materials. A further goal to achieve ALD grown materials with permittivities above 100 and minimal leakage current densities, either in their as-deposited form or after post-processing treatments. For dielectric films with compositions known to be ferroelectric in bulk ceramics and and thick films, it was also of interest to achieve ferroelectric properties.

The first ever ALD growth results for $SrTiO_3$, $BaTiO_3$, $Ba_{(1-x)}Sr_xTiO_3$ and $BiTaO_4$ were reported. Of these processes, the alkaline earth metal titanate deposition processes have since proved robust enough for large area (200 mm wafer) processing in industrial pilot experiments.[196] For $SrTa_2O_6$ it was found that bimetallic alkoxides can be used as the precursors in self-limiting growth reactions with H_2O as the oxygen source. Preparation of ferroelectric capacitors by ALD with separate metal precursors was for the first time demonstrated for $SrBi_2Ta_2O_9$ and $Bi_4Ti_3O_{12}$.

Permittivities above 100 were observed for $SrTiO_3$, $BaTiO_3$, $Ba_{(1-x)}Sr_xTiO_3$ and $Bi_4Ti_3O_{12}$ after post-annealing, and permittivies around 90 for low-temperature grown as-deposited $SrTiO_3$ films. A high permittivity value of 280 was obtained for a 140 nm thick $BaTiO_3$ film annealed at 800 °C. Leakage currents below $1.0 \cdot 10^{-7}$ A/cm^2 were achieved at 1 volt bias for 32 nm $BaTiO_3$, 54 nm BST and 51 nm $Bi_4Ti_3O_{12}$ films when these were annealed in oxygen atmospheres with high work function Pt electrodes. For films thinner than 30 nm, the roughness of the electrode–dielectric interfaces most likely begins to dominate the overall leakage. The lowest EOT achieved in this study was 1.08 nm at 1 V bias for a 35 nm BST film, with a leakage current level of 10^{-5} A/cm^2 at the same voltage.

All materials required post-annealing treatment in order to reach permittivity values above 100. Improvements in dielectric properties can be expected with improved bottom electrode materials, namely, either extremely smooth metal films or lattice-matched materials such as $SrRuO_3$. With well-matched electrode materials, epitaxial and fully surface controlled ALD growth of materials such as $SrTiO_3$ may be possible. Such electrode layers are unlikely to be available in devices in the near future, however.

Reports in the literature clearly show that RTA methods are critically necessary for the preparation of ferroelectric materials $SrBi_2Ta_2O_9$ and $Bi_4Ti_3O_{12}$. RTA methods should in future be applied to ALD grown films in order to obtain the best possible results for the small-grained sub-50 nm films that already are needed in microelectronics.

Much will be gained with improved ALD precursors. Improved sources for Ti and Bi are perhaps the most critical need for the preparation of the materials studied here, at the time of this study. The single most important prerequisite for fruitful development of multicomponent oxide ALD is the availability of a range of appropriate ALD precursors.

Refererences

1. T. Suntola, *Thin Solid Films*, **216**, (1992), 84

2. H. Seidl, M. Gutsche, U. Scroeder, A. Birner, T. Hecht, S. Jakschik, J. Luetzen, M. Kerber, S. Kudelka, T. Popp, A. Orth, H. Reisinger, A. Saenger, K. Schupke and B. Sell, *IEDM Tech. Dig.* (2002), 839

3. J.M. Hergenrother, G.D. Wilk, T. Nigam, F.P. Klemens, D. Monroe, P.J. Silverman, T.W. Sorsch, B. Busch, M.L. Green, M.R. Baker, T. Boone, M.K. Bude, N.A. Ciampa, E.J. Ferry, A.T. Fiory, S.J. Hillenius, D.C. Jacobson, R.W. Johnson, P. Kalavade, R.C. Keller, C.A. King, A. Kornblit, H.W. Krautter, J.T.-C. Lee, W.M- Mansfield, J.F. Miner, M.D. Morris, S.-H. Oh, J.M. Rosamilia, B.J. Sapjeta, K. Short, K. Steiner, D.A. Muller, P.M. Voyles, J.L. Grazul, E.J. Shero, M.E. Givens, C. Pomarede, M. Mazanec and C. Werkhoven, *IEDM Tech. Dig.* (2001), 51

4. M. Kemell, V. Pore, M. Ritala, M. Leskelä and Mika Lindén, *J. Am. Chem. Soc.*, **127**, (2005), 14179

5. M.Ritala and M. Leskelä, *Handbook of Thin Film Materials*; Nalwa, H. S. Ed.; Academic Press: New York, Vol. 1. pp 103-125 (2002)

6. J.W. Elam, D. Routkevich, P.P. Mardilovich and S. M. George, *Chem. Mater*. 15, (2003), 3507

7. M. Ritala, M. Kemell, M. Lautala, A. Niskanen, M. Leskelä and S. Lindfors. *Chem. Vap. Deposition* 12, (2006), 655

8. M. Juppo, M. Vehkamäki, M. Ritala and M. Leskela, *J. Vac. Sci. Technol*. A. 16, (1998), 2845

9. T. Hatanpää, M. Vehkamäki, I- Mutikainen, J. Kansikas, M. Ritala and M. Leskelä, *Dalton Trans*. (2004) 1181

10. J. Harjuoja, T. Hatanpää, M. Vehkamäki, S. Väyrynen, M. Putkonen, L. Niinistö, M. Ritala, M. Leskelä, E. Rauhala, *Chem. Vap. Deposition*, **11**, (2005), 362

11. M. Schuisky, K. Kukli, M. Ritala, A. Hårsta, M. Leskelä, *Chem. Vap. Deposition*, **6**, (2000), 139

12. G. W. Hwang, W.D. Kim, Y-S. Min, Y. J. Cho and C. S. Hwang, *J. Electrochem. Soc.* **153**, (2006), F20-F26

13. J. Harjuoja, S. Väyrynen, M. Putkonen, L. Niinistö, E. Rauhala, *J. Cryst. Growth* **286**, (2006), 376

14. G.W. Hwang, W.D. Kim, C. S. Hwang, Y.-S. Min and Y. J. Cho, J. Electrochem Soc. **154**, (2007), H915

15. M-Y. Ho, H. Gong, G.D. Wilk, B.W. Busch, M.L. Green, W.H. Lin, A. See, S.K. Lahiri, M.E. Loomans, P. I. Räisänen, T. Gustafsson, *Appl. Phys. Lett.*, **81**, (2002), 4218

16. S-H. Kim and S-W. Rhee, *Chem. Vap. Deposition*, **12**, (2006), 125

17. K. Kukli, M. Ritala, M. Leskelä, T. Sajavaara, J. Keinonen, R. I. Hegde, D. C. Gilmer, P. J. Tobin, *J. Electrochem. Soc.* **151**, (2004), F98

18. Z. M. Rittersma, F. Roozeboom, M. A. Verheijen, J.G.M. van Berkum, T. Dao, J.H.M. Snijders, E. Väinönen-Ahlgren, E. Tois, M. Tuominen, S. Haukka, *J. Electrochem. Soc.* **151**, (2004), C716-C722

19. M. Nieminen, T. Sajavaara, E. Rauhala, M. Putkonen and L. Niinistö, *J. Mater. Chem.* **11**, (2001), 2340

20. H. Seim, M. Nieminen, L. Niinistö, H. Fjällvåg, L-S. Johansson, *Appl. Surf. Sci.*, **112** (1997) 243

21. M. Nieminen, S. Lehto and L. Niinistö, *J. Mater. Chem.* **11**, (2001),3148

22. O. Nilsen, M. Peussa, H. Fjellvåg, L. Niinistö and A. Kjekshus, *J. Mater. Chem.* **9**, (1999), 1781

23. H. Seim, H. Mölsä, M. Nieminen, H. Fjellvåg and L. Niinistö, *J. Mater. Chem.***7**, (1997), 449

24. M. Putkonen, M. Nieminen and L. Niinistö, *Thin Solid Films*, **466**, (2004), 103

25. A. Kosola, J. Päiväsaari, M. Putkonen and L. Niinistö, *Thin Solid Films*, **479** (2005), 152

26. J. Harjuoja, A. Kosola, M. Putkonen and L. Niinistö, *Thin Solid Films*, **496**, (2006), 346

27. G. W. Hwang, H. J. Lee, K. Lee and C. S. Hwang, *J. Electrochem. Soc.* **154**, (2007), G69

28. J. Harjuoja, S. Väyrynen, M. Putkonen, L. Niinistö and E. Rauhala, *Appl. Surf. Sci.* **253**, (2007), 5228

29. W.-J. Lee, I.-K. You, S.-O. Ryu, B.-G. Yu, K.-I. Cho, S.-G. Yoon and C.-S. Lee, *Jpn. J. Appl. Phys., Part 1*, **40**, 6941 (2001)

30. D.-S. Kil, J.-M. Lee and J.-S. Roh, *Chem. Vap. Deposition* **8**, (2002), 195

31. A. Kosola, M. Putkonen, L.-S. Johansson and L. Niinistö, *Appl. Surf. Sci.* **211** (2003) 102-112

32. O. S. Kwon, S. K. Kim, M. Cho, C. S. Hwang and J. Jeong, J. Electrochem Soc. **152**, (2007), C229

33. H. Kattelus, M. Ylilammi, J. Saarilahti, J. Antson and S. Lindfors, *Thin Solid Films*, **225**,(1993), 296

34. K. Kukli, M. Ritala and M. Leskelä, *Nanostructured Materials* **8**, (1997), 785

35. P. Myllymäki, M. Nieminen, J. Niinistö, M. Putkonen, K. Kukli and L. Niinistö, *J. Mater. Chem.* **16**, (2006), 563

36. M. Ritala, K.Kukli, A. Rahtu, P.I. Räisänen, M. Leskelä, T. Sajavaara, J. Keinonen, *Science*, **288**, (2000), 319

37. K. Kukli, M. Ritala, M. Leskelä, T. Sajavaara, J. Keinonen, D. Gilmer, S. Bagchi, and L. Prabhu, *Journal of Non-Crystalline Solids* **303**, (2002), 35

38. Z. M. Rittersma, E. Naburgh, T. Dao, A.H.C. Hendriks, W.F.A. Besling, E. Tois, E. Vainonen-Ahlgren, M. Tuominen and S. Haukka, *Electrochem. Solid-State Lett.* **6**, (2003), F21-F23

39. A. Rahtu, M. Ritala and M. Leskelä, *Chem. Mater.* **13**, (2001), 1528

40. Y. J. Cho, Y.-S. Min, J.-H. Lee, B.-S. Seo, J.K. Lee, Y.S. Park, *Integr. Ferroelectr.* **59**, (2003), 1483

41. Y.-S. Min, I. P. Asanov and C. S. Hwang, Electrochem. Solid-State Lett. **9**, (2006), G231

42. Y.-S. Min, Y.J. Cho, I. P. Asanov, J. H. Han, W. D. Kim and C. S. Hwang, *Chem. Vap. Deposition* **11**, (2005), 38

43. J. H. Lee, Y. J. Cho, Y.S. Min, D. Kim and S.W. Rhee, *J. Vac. Sci. Technol. A* **20**, (2002), 1828

44. W. C. Shin, S.O. Ryu, I. K. You, S. M. Yoon, S. M. Cho, N.Y. Lee, K.D. Kim, B.G. Yu, W.J. Lee, K. J. Choi and S.G. Yoon, *Electrochem. Solid-state Lett.* **7**, (2004), F31

45. A.I. Kingon, J-P. Maria and S.K. Streiffer, *Nature*, **406** (2000), 1032

46. J. Robertson, *Rep. Prog. Phys.* **69** (2006) 327

47. C.S. Hwang, J. Appl. Phys. **92**, (2002), 432

48. M. Stengel and N. A. Spaldin, Nature **443**, (2006),679

49. S. K. Singh, Y.K. Kim, H. Funakubo and H. Ishiwara, *Appl. Phys. Lett.* **88**, (2006), 162904

50. R. D. Shannon, *Acta Cryst. A* **32,** (1976), 751

51. M. Valant and P. K. Davies, *J. Am. Ceram. Soc.* **83**, (2000), 147

52. K. Xiong and J. Robertson, *Appl. Phys. Lett.* **85** (2004), 2577

53. P. W. Peacock and *Appl. Phys. Lett*, **83**, (2003), 2025

54. A.R. West, *Solid State Chemistry an Its Applications*, Wiley (1984), pp. 204-207

55. T. Sato, D. Noréus, H. Takeshita, and U. Häussermann, *J. Solid State Chem.* **178**, (2005), 3381

56. V.V. Lemanov, A.V. Sotnikov, E.P. Smirnova, M. Weihnacht and R. Kunze, *Solid State Comm.* **110**, (1999), 611

57. K. A. Müller and H. Burkard, *Phys. Rev. B.* **19**, (1979), 3593

58. J. H. Haeni, P. Irvin, W. Chang, R. Uecker, P. Reiche, Y. L. Li, S. Choudbury, W. Tian, M.E. Hawley, B. Craigo, A. K. Tagantsev, X. Q. Pan, S. K. Streiffer, L. Q. Chen, S. W. Kirchoefer, J. Levy, D. G. Schlom, *Nature*, **430**, (2004), 758

59. B. C. Frazer, H.R. Danner and R. Pepinsky, *Phys. Rev.* **100**, (1955), 745

60. B. Aurivillius, *Ark. Kemi.***1**, (1949), 463

61. Y. Shimakawa, Y. Kubo, Y. Nakagawa, S. Goto, T. Kamiyama, H. Asano and F. Izumi. *Phys. Rev. B.* **61**, (2000), 6559

62. Y. Shimakawa, Y. Kubo, Y. Nakagawa, T. Kamiyama, H. Asano and F. Izumi, *Appl. Phys. Lett.* **74**, (1999), 1904

63. C. H. Hervoches and P. Lightfoot, *Chem. Mater.* **11**, (1999), 3359

64. Y. Shimakawa, Y. Kubo, Y. Tauchi, H. Asano, T. Kamiyama, F. Izumi and Z. Hiroi, *Appl. Phys. Lett.* **79**, (2001), 2791

65. B. H. Park, B. S. Kang, S.D. Bu, T.W. Noh, J. Lee and W. Jo, *Nature*, **401**, (1999), 682

66. C.H. Hervoches and P. Lightfoot, *J. Solid State Chem.* **153**, (2000), 66

67. T. J. Boyle, C.D. Buchheit, M. A. Rodriguez, H. N. Al-Shareef, B. A. Hernandez, B. Scott and J. W. Ziller, *J. Mater. Res.* **11**, (1996), 2274

68. M. A. Rodriguez, T. J. Boyle and B.A. Hernandez, *Advances in X-Ray Analysis*, **41**, (1999), 28

69. J. S. Lee, H.J. Kwon, Y. W. Jeong, H.H. Kim, S.J. Hyun and T.W. Noh, *Appl. Phys. Lett.* **74**, (1999), 2690

70. Y-M. Sung, W-C. Kwak, *Chem. Phys. Lett.* **411**, (2005), 389

71. D.P. Cann, C. A. Randall and T. R. Shrout, *Solid State Comm.* **100**, (1996), 529

72. M.A. Rodriguez, T.J. Boyle, B.A.Hernandez, C. D. Buchheit and M.A. Eatough, *J. Mater. Res.*, **11**, (1996), 2282

73. S.-Y. Chen, B.-C. Lan, C.-S. Taso and S.-Y. Lee, *J. Non-crystalline solids*, **320**, (2003), 76

74. A.L. Hector and S. B. Wiggin, *J. Solid State Chem.* **177**, (2004), 139

75. I. Radosavljevic, J. S. O. Evans and A. W. Sleight, *J. Solid State Chem.* **136**, (1998), 63

76. B. Nguyen, Y. Liu and R. L. Withers, *J. Solid. State Chem.* **180**, (2007), 549

77. H. Schroeder, A. Kingon, *Nanoelectronics and Information Technology*; R. Waser Ed., Wiley-VCH (2003) p. 540-561

78. J. Y.-M. Lee and B. C. Lai, *Handbook of Thin Film Materials*; Nalwa, H. S. Ed.; Academic Press: New York, Vol. 3. pp 2-100 (2002)

79. D. Roberts, W. Johnstone, H. Sanchez, O. Mandhana, D. Spilo, J. Hayden, E. Travis, B. Melnick, M. Celik, B. W. Min, J. Edgerton, M. Raymond, E. Luckowski, C. Happ, A. Martinez, B. Wilson, P. Leung, T. Garnett, D. Goedeke, T. Remmel, K. Ramakrishna and B.E. White, *IEDM Tech. Dig.* (2005), 77

80. N. Inoue, H. Ohtake, I. Kume, N. Furutake, T. Onodera, S. Saito, A. Tanabe, M. Tagami, M. Tada and Y. Hayashi, *IITC Proceedings*, (2006), 63

81. H.S. Kim, D.H. Kim, J.M. Park, Y.S. Hwang, M. Huh, H.K. Hwang, N.J. Kang, B.H. Lee, M.H. Cho, S.E. Kim, J.Y. Kim, B.J. Park, J. W. Lee, D.I. Kim, M.Y. Jeong, H.J. Kim, Y.J. Park and K. Kim, *IEDM Tech. Dig* (2003), 411

82. K.U. Stein, A. Sihling and E. Doering, *ISSCC Digest of Technical papers*, (1972), 56

83. S. Suzuki, M. Nakao, T. Takeshima, M. Yoshida, M. Kikuchi and K. Nakamura, *ISSCC Digest of Technical papers*, (1984), 106

84. Y. Takamae, T. Ema, M. Nakano, F. Baba, T.Yabu, K. Miyasaka, K. Shirai, *ISSCC Digest of Technical papers*, (1985), 250

85. M.K. Choi, B.-G. Jeon, N. Jang, B.-J. Min, Y.-J. Song, S.-Y. Lee, H. H. Kim, D.-J. Jung, H.-J. Joo, K. Kim, *ISSCC Digest of Technical papers*,(2002), 162

86. H. Kohlstedt, Y. Mustafa, A. Gerber, A. Petraru, M.Fitsilis, R. Meyer, U. Böttger and R. Waser, *Microelectron. Eng.* **80**, (2005), 296

87. M. Ylilammi and T. Ranta-aho, *Thin Solid Films*, **232**,(1993),56

88. R.A. Waldo, *Microbeam Anal.* (1988), 310

89. C. Sawyer and C. Tower, *Phys. Rev.* **35**,(1930), 269

90. S. K. Kim, W.-D. Kim, K.-M. Kim, C. S. Hwang and J. Jeong, *Appl. Phys. Lett.* **85**, (2004), 4112

91. M. Ritala and M. Leskelä, *Chem. Mater.* **5**, (1993), 1174

92. V. Pore, A. Rahtu, M. Leskelä, M. Ritala, T. Sajavaara and J. Keinonen, *Chem.Vap. Deposition* **3**, (2004), 10

93. F.-C. Chiu, J.-J. Wang, J. Y.-M. Lee and S. C. Wu, *J. Appl. Phys.* **81**, (1997), 6911

94. J. Lin, N. Masaaki, A. Tsukune and M. Yamada, *Appl. Phys. Lett.* **74**, (1999), 2370

95. K. Kukli, M. Ritala and M. Leskelä, *J. Electrochem. Soc.* **142**, (1995), 1670

96. M. Pessa, R. Mäkelä and T. Suntola, *Appl. Phys. Lett.* **38**, (1981), 131

97. J. Sundqvist, H. Högberg and A. Hårsta, *Chem. Vap. Deposition*, **9**,(2003), 245

98. H. S. Booth and L. H. McIntyre, *Ind. Eng. Chem., Anal. Ed.* **2**, (1930) 12

99. F. Trusell and H. Diehl, *Anal. Chem.* **6**, (1963), 674

100. D.R. Mueller, R.L. Kurtz, R.L. Stockbauer and T.E. Madey, *Surf. Sci.* **237**, (1990), 72

101. D. H. Baker, R. L. Champion and L. D. Doverspike and Y. Wang, *Appl. Phys. Lett.* **64**, (1994), 1880

102. N. Takahashi, H. Shinjoh, T. Iijima, T. Suzuki, K. Yamazaki, K. Yokota, H. Suzuki, K. Yamazaki, K. Yokota, H. Suzuki, N. Miyoshi, S.-I. Matsumoto, T. Tanizawa, T. Tanaka, S.-S. Tateishi and K. Kasahara, *Catalysis Today* **27**, (1996), 63

103. K. Kukli, M. Ritala, T. Sajavaara, T. Hänninen and M. Leskelä, *Thin Solid Films*, **500**, (2006), 322

104. Y. Kado and Y. Arita, *J. Appl. Phys.* **61**, (1987), 2398

105. R. A. McKee, F. J. Walker and M.F. Chisholm, *Phys. Rev. Lett.* **81**, (1998), 3014

106. K. Eisenbeiser, J.M. Finder, Z. Yu, J. Ramdani, J. A. Curless, J. A. Hallmark, R. Droopad, W. J. Ooms, L. Salem, S. Bradshaw and C. D. Overgaard, *Appl. Phys. Lett.* **76**, (2000), 1324

107. J.A. Switzer, M.G. Shumsky and E.W. Bohannan, *Science*, **284**, (1999), 293

108. M. Schuisky and A. Hårsta, *Chem. Vap. Deposition* **2**, (1996),235

109. D.E. Sparks, P. M. Patterson, G. Jacobs, M. Crocker and J. A. Chaney, *Catalysis Communications*, **7**, (2006),122

110. T. A. Hanna, *Coordin. Chem. Rev.* **248**, (2004), 429

111. K. A. Müller and H. Burkard, *Phys. Rev. B* **19**, (1979), 3593

112. P. Kuzel, F. Kadlec, H. Nemec, R. Ott, E. Hollmann and N. Klein, *Appl. Phys. Lett.* **88**, (2006), 102901

113. A.T. Findikoglu, Q.X. Jia, I.H. Campbell, X.D. Wu, D. Reagor, C.B. Mombourquette and D. McMurry, *Appl. Phys. Lett.* **66**, (1995), 3674

114. R. C. Neville, B. Hoeneisen and C. A. Mead, *J. Appl. Phys.* **43**, (1972), 2124

115. H.-M. Christen, J. Mannhart, E.J. Williams and Ch. Gerber, *Phys. Rev. B*, **49**, (1994), 12095

116. W.A. Feil, B.W. Wessels, L.M. Tonge and T.J. Marks, *J. Appl. Phys.* **67**,(1990), 3858

117. T. Maeda, G.H. Lee, T. Ohnishi, M. Kawasaki, M. Yoshimoto and H. Koinuma, *Mat. Sci. Eng.* **B41**, (1996), 134

118. H.-C. Li, W. Si, A.D. West and X.X. Xi, *Appl. Phys. Lett.* **73**, (1998), 190

119. M. Klee, U. Mackens, *Microelectron. Eng.* **29** (1995), 185

120. G. W. Dietz, W. Antpöhler, M. Klee, R. Waser, *J. Appl. Phys.* **78**, (1995), 6113

121. G. J. Norga, C. Marchiori, C. Rossel, A. Guiller, J.P. Locquet, H. Siegwart, D. Caimi, J. Fompeyrine, J.W. Seo and Ch. Dieker, *J. Appl. Phys.* **99**, (2006), 084102

122. M. Stengel and N. A. Spaldin, *Nature*, **443**, (2006), 679

123. N. H. Finstrom, J. Cagnon and S. Stemmer, *J. Appl. Phys.* **101**, (2007), 034109

124. J. Ihanus, T. Hänninen, T. Hatanpää, M. Ritala and M. Leskelä, *J. Electrochem. Soc.* **151**, (2004), H221

125. M. Linnermo and M. Vehkamäki, unpublished results

126. M. Vehkamäki, T. Hänninen, M. Ritala, M. Leskelä, R. Droopad, J. Ramdani, D. Gilmer and J. Yu, presented at the TFDOM 2 conference (2001)

127. M. Kiyotoshi and K. Eguchi, *Appl. Phys. Lett.* **67**, (1995), 2468

128. A. von Hippel, *Rev. Mod. Phys*. **22**, (1950), 221

129. S. Fujishima, *IEEE Transactions on Ultrasonics, Ferroelectrics and Frequency Control*, **47**, (2000), 1

130. G.H. Haertling, *J. Am. Ceram. Soc.* **82**, (1999), 797

131. B. Heinen and R. Waser, *J. Mater. Sci.* **33**, (1998), 4603

132. N. A. Pertsev, A. G. Zembilgotov, S. Hoffmann, R. Waser and A. K. Tagantsev, *J. Appl. Phys.* **85**, (1999), 1698

133. Y.S. Kim, J.Y. Jo, D.J. Kim, Y.J. Chang, J.H. Lee and T.W. Noh, T.K Song, J.-G. Yoon, J.-S Chung, S. I. Baik, Y.-W.Kim and C. U. Jung, *Appl. Phys. Lett.* **88**, (2006), 072909

134. K.J. Choi, M. Biegalski, Y.L. Li, A. Sharan, J. Schupert, R. Uecker, P. Reiche, Y.B. Chen, X.Q. Pan, V. Gopalan, L.-Q. Chen, D.G. Schlom and C.B. Eom, *Science*, **306**, (2004), 1005

135. J. W. Jang, S. J. Chung, W.J. Cho, T. S. Hahn and S. S. Choi, *J. Appl. Phys.* **81**, (1997), 6323

136. L. Beckers, J. Schubert, W. Zander, J. Ziesmann, A. Eckau, P. Leinenbach and Ch. Buchal, *J. Appl. Phys.* **83**, (1997), 3305

137. R.W. Schwartz, *Chem. Mater.* **9**, (1997), 2325

138. B.S. Kwak, K. Zhang, E. P. Boyd, A. Erbil and B. J. Wilkens, *J. Appl. Phys.* **69**, (1991), 767

139. K. Sreenivas, A. Mansingh and M. Sayer, *J. Appl. Phys.* **62**, (1987), 4475

140. P. Gonon and F. El Kamel, *J. Appl. Phys.* **101**, (2007), 073901

141. C. S. Hwang, Mat. Sci. Eng. **B56**, (1998), 178

142. S. Ezhilvalavan and T.-Y.Tseng, *Mat. Chem. Phys.* **65**, (2000), 227

143. M. Nayak, S. Ezhilvalavan and T.-Y. Tseng, *Handbook of Thin Film Materials*; Nalwa, H. S. Ed.; Academic Press: New York, Vol. 3. pp 100-160 (2002)

144. P. Padmini, T.R. Taylor, M.J. Lefevre, A.S. Nagra, R.A. York and J.S. Speck, *Appl. Phys. Lett.* **75**, (1999), 3186

145. C. S. Hwang, S. O. Park, H.-J. Cho, C. S. Kang, H.-K. Kang, S. I. Lee and M. Y. Lee, *Appl. Phys. Lett.* **67**, (1995), 2819

146. B.A. Baumert, L.H. Chang, A.T. Matsuda, T.-L. Tsai, C.J. Tracy, R.B. Gregory, P.L. Fejes, N.G. Fejes, N.G. Cave and W. Chen, *J. Appl. Phys.* **82**, (1997), 2558

147. S. Regnery, P. Ehrhart, F. Fitsilis, R. Waser, Y. Ding, C.L. Jia, M. Schumacher, F. Schienle and H. Juergensen, *J. Eur. Ceram. Soc.* **24**, (2004), 271

148. C.S. Chern, S. Liang, Z.Q. Shi, S. Yoon, A. Safari, P. Lu, B.H. Kear, B.H. Goodreau, T.J. Marks and S. Y. Hou, *Appl. Phys. Lett.* **64**, (1994), 3181

149. U. Hasenkox, S. Hoffman and R. Waser, *J. Sol-Gel Science Technol.* **12**, (1998), 67

150. S.-G. Yoon, J.-C. Lee and A. Safari, *J. Appl. Phys.* **76**, (1994), 2999

151. C. Basceri, S.K Streiffer, A. I. Kingon and R. Waser, *J. Appl. Phys.* **82**, (1997), 2497

152. T.M. Shaw, Z. Suo, M. Huang, E. Liniger, R.B. Laibowitz and J. D. Baniecki, *Appl. Phys. Lett.* **75**, (1999), 2129

153. M. A. Rodriguez, T. J. Boyle, B. A. Hernandez, D. A. Tallant and K. Vandeusden, *J. Am. Ceram. Soc.* **82**, (1999), 2101

154. R. J. Potter, P. A. Marshall, J. L. Roberts, A. C. Jones, P. R. Chalker, M. Vehkamäki, M. Ritala, M. Leskelä, P.A. Williams, H. O. Davies, N. L. Tobin and L. M. Smith, *MRS Proceedings*, **784**, (2003), 97

155. D.-O. Lee, P. Roman, C.-T. Wu, W. Mahoney, M. Horn, P. Mumbauer, M. Brubaker, R. Grant and J. Ruzyllo, *Microelec. Eng.* **59**, (2001), 405

156. S. Regnery, R. Thomas, P. Ehrhart and R. Waser, *J. Appl. Phys.* **97**, (2005), 073521

157. L. Goux, H. Vander Meeren and D.J. Wouters, *J. Electrochem. Soc.* **153**, (2006), F132

158. L. Goux and D.J. Wouters, *J. Appl. Phys.* **100**, (2006), 126103

159. C.-L. Huang and M-H. Weng, *Mater. Lett.* **43**, (2000), 32

160. M. Lim, V. Joshi, S. Narayan, J. Celinska and J. Karasawa, *Appl. Phys. Lett.* **81**, (2002), 1863

161. C.-Y. Lee, R. Macquart, Q. Zhou and B. J. Kennedy, *J. Solid State Chem.* **174**, (2003), 310

162. J.F. Scott, *Science*, **315**, (2007), 954

163. C. A. Paz de Araujo, J. D. Cuchiaro, L. D. McMillan, M. C. Scott and J.F. Scott, *Nature*, **374**, (1995), 627

164. J. Celinska, V. Joshi, S. Narayan, L. McMillan and C. Paz de Araujo, *Appl. Phys. Lett.* **82**, (2003), 3937

165. J. A. Johnson, J. G. Lisoni and D. J. Wouters, *Microelec. Eng.* **70**, (2003), 377

166. D.J. Wouters, D. Maes, L. Goux, J. G. Lisoni, V. Paraschiv, J. A. Johnson, M. Schwitters, J.-L. Everaert, W. Boullart, M. Schaekers, M. Willegems, H. Vander Meeren and L. Haspeslagh, C. Artoni, C. Caputa, P. Casella, G. Corallo, G. Russo, R. Zambrano, H. Monchoix, G. Vecchio and L. Van Autryve, *J. Appl. Phys.* **100**, (2006), 051603

167. H. N. Lee, A. Visinoiu, S. Senz, C. Harnagea, A. Pignolet, D. Hesse and U. Gösele, *J. Appl. Phys.* **88**, (2000), 6658

168. R. Iijima, *Appl. Phys. Lett.* **79**, (2001), 2240

169. K. Amanuma, T. Hase and Y. Miyasaka, *Appl. Phys. Lett.* **66**, (1995), 221

170. M.L. Calzada, R. Jimenez, A. Gonzales and J. Mendiola, *Chem. Mater.* **13**, (2001), 3

171. T. Li, Y. Zhu, S. B. Desu, C.-H. Peng and M. Nagata, *Appl. Phys. Lett.* **68**, (1996), 616

172. C.G. Condorelli, M. Favazza, C. Bedoya, A. Baeri, G. Anastasi, R. Lo Nigro, N. Menou, C. Muller. J.G. Lisoni, D. Wouters and I. L. Fragala, *Chem. Mater.* **18**, (2006), 1016

173. L. Goux, J.G. Lisoni. M. Schwitters, V. Paraschiv, D. Maes, L. Haspeslagh, D.J. Wouters, N. Menou, Ch. Turquat, V. Madigou, Ch. Muller and R. Zambrano, *J. Appl. Phys.* **98**, (2005), 054507

174. R. Dat, J.K. Lee, O. Auciello and A.I. Kingon, *Appl. Phys. Lett.* **67**, (1995), 572

175. S. Zhang, Y. Li, W. Fei, Z. Gan, S. Mhaisalkar and X.M. Li, *J. Vac. Sci. Technol.* A **24**, (2006), 1992

176. M. Calzada, A. Gonzalez, J. Garcia-Lopez and R. Jimenez, *Chem. Mater.*, **15** (2003), 4775

177. J. S. Lee, H. H. Kim, H. J. Kwon and Y. W. Jeong, *Appl. Phys. Lett.* **73**, (1998), 166

178. S.-Y. Jung, S.-J. Hwang and Y.-M. Sung, *J. Mater. Res.* **18**, (2003), 1745

179. S.E. Cummins and L. E. Cross, *J. Appl. Phys.* **39**, (1968), 2268

180. W. Jo, G.-C. Yi, T.W. Noh, D.-K. Ko, Y.S. Cho and S.-I. Kwun, *Appl. Phys. Lett.* **61**, (1992), 1516

181. A. Megriche, L. Lebrun and M. Troccaz, *Sensors and Actuators*, **78**, (1999), 88

182. K. Sugibuchi, Y. Kurogi and N. Endo, J. Appl. Phys. **46**, (1975), 2877

183. E. Rokuta, Y. Hotta, T. Kubota, H. Tabata, H. Kobayashi and T. Kawai, *Appl. Phys. Lett.* **79**, (2001), 403

184. B.-E. Park, K. Takahashi and H. Ishiwara, *Appl. Phys. Lett.* **85**, (2004), 4448

185. W. Li, A. Chen, X. Lu and J. Zhu, *J. Appl. Phys.* **98**, (2005), 024109

186. T.-Y. Chiou and D.-H. Kuo, *Appl. Phys. Lett.* **85**, (2004), 3196

187. T. Watanabe, H. Funakubo, M. Osada, Y. Noguchi and M. Miyayama, *Appl. Phys. Lett.* **80**, (2002), 100

188. S. K. Singh and H. Ishiwara, *Solid State Comm.* **140**, (2006), 430

189. R. Ramesh, K. Luther, B. Wilkens, D.L. Hart, E. Wang, J. M. Tarascon, A. Inam, X. D. Wu and T. Venkatesan, *Appl. Phys. Lett.* **57**, (1990), 1505

190. W. J. Takei, N.P. Formigoni and M.H. Francombe, *Appl. Phys. Lett.* **15**, (1969), 256

191. S. Choopun, T. Matsumoto and T. Kawai, *Appl. Phys. Lett.* **67**, (1995), 1072

192. J. Si and S. B. Desu, *J. Appl. Phys.* **73**, (1993), 7910

193. T. Watanabe, A. Saiki, K. Saito and H. Funakubo, *J. Appl. Phys.* **89**, (2001), 3934

194. M. Schuisky, A. Hårsta, S. Khartsev and A. Grishin, *J. Appl. Phys.* **88**, (2000), 2819

195. P.C. Joshi, A. Mansingh, M. N. Kamalasanan and S. Chandra, *Appl. Phys. Lett.* **59**, (1991), 2389

196. R. Matero, A. Rahtu, S. Haukka, M. Tuominen, M. Vehkamäki, T. Hatanpää, M. Ritala and M. Leskelä, *ECS Transactions* **1**, (2006), 137